Applied Surface Science Advances 18 (2023) 100520

Contents lists available at ScienceDirect

Applied Surface Science Advances

journal homepage: www.sciencedirect.com/journal/applied-surface-science-advances

A review of recent progress in solar fuel (Hydrogen) generation *via* photocatalytic water-splitting of cadmium sulfide (CdS) based photocatalyst

Dahiru Umaru [a,b], Hafeez Yusuf Hafeez [b,*], J. Mohammed [b], Abdussalam Balarabe Suleiman [b], Chifu Ebenezer Ndikilar [b], Yusuf Zakariyya [a]

[a] *Department of Physics, Faculty of Science, Yobe State University, P.M.B 1144, Kashim Ibrahim way, Damaturu, Yobe, Nigeria*
[b] *Department of Physics, Faculty of Science, Federal University Dutse, P.M.B 7156, Ibrahim Aliyu By Pass, Jigawa, Nigeria*

ARTICLE INFO

Keywords:
Cadmium Sulfide
Z-Scheme
S-Scheme
Solar fuel
Hydrogen
Photocatalyst

ABSTRACT

Globally, energy demand and environmental pollution affect the development of society. However, solar fuel generation via photocatalytic water-splitting became the most viable approach to address the global energy crisis. Cadmium sulfide is considered an ideal material for solar fuel (hydrogen) generation due to its promising, low-cost, suitable bandgap energy, desired band alignment, affordability, and simple preparation method. However, the solar-to-hydrogen (STH) conversion efficiency of CdS-based materials still needs to improve due to the high rate of photogenerated electron-hole pair recombination and photocorrosion, resulting in poor photocatalytic performance. Herein, an emerging approach for enhancing the stability and photocatalytic activity of CdS is discussed, including designing heterostructure, co-catalyst loading, etc., with a focus on charge carrier separation and transfer. Particular attention is given to the mechanism of the emerging approach that influences photocatalytic water-splitting. This review focuses on designing and developing of strategy for enhancing anti-photocorrosion CdS-based materials for solar fuel generation. Notably, the solar H_2 production improvements achieved in studying the CdS material as the main photocatalyst, not a co-catalyst, were exclusively reviewed and discussed. The prospective, challenges and development in preparation for anti-photo corrosion CdS are discussed. Thus, this review would likely motivate researchers to broaden the applications for CdS-based materials in solar fuel (hydrogen) generation in an economical and eco-friendly approach.

1. Introduction

There is a worldwide emphasis on the importance of energy consumption as a basic necessity for human daily activities. However, the reliability of energy security provided by fossil fuels, which are carbon-based, is being questioned due to their depletion and their association with greenhouse gasses (GHG), water pollution, energy security concerns, global warming, and climate change. As an alternative energy source, hydrogen (H_2) is considered a renewable option to replace fossil fuels, which currently account for 80% of the world's energy demand. Hydrogen is considered pollution-free because it does not contain CO_2 when combusted, has 0.08988 g/L density at standard temperature and pressure (STP), and is lighter in comparison with other fuels e.g., natural gas and ethanol [1,2]. Moreover, the highest energy content of H_2 is ~140 MJ/kg compared to other fuels and can be produced from an abundant source i.e. water [3]. Economically, H_2 is extensively considered and widely gained acceptance as an alternative fuel due to its excellent properties in terms of renewability and free-pollution characteristics to address the global energy security concerns regarding environmental issues, energy availability, prices, societal effects, etc., [4]. Also, H_2 is considered a most promising candidate for solar fuel conversion and storage though its production is accompanied by many challenges both scientific and technical which obstruct its worldwide implementation [2]. Therefore, producing H_2 *via* photocatalytic water-splitting has become the most viable approach to address global energy demands and environmental pollution.

Single photocatalysts exhibit low photocatalytic H_2 production due to fast charge carrier recombination, wide band gap, and photocorrosion [5]. Several research work has been carried out to address the problem associated with single photocatalysts such as TiO_2, CdS, and g-C_3N_4 [6].

* Corresponding author.
E-mail address: hafeez.y@fud.edu.ng (H.Y. Hafeez).

https://doi.org/10.1016/j.apsadv.2023.100520
Received 23 September 2023; Received in revised form 23 November 2023; Accepted 23 November 2023
Available online 5 December 2023
2666-5239/© 2023 The Authors. Published by Elsevier B.V. This is an open access article under the CC BY license (http://creativecommons.org/licenses/by/4.0/).

Irrespective of the potentiality of semiconductors in photocatalysts, their practical use is constrained by a number of problems such as inefficient usage of sunlight, poor quantum yield, charge carrier recombination [7]. For example, Pristine CdS is an n-type material that attracted much attention of researchers because of its excellent properties such as the efficient charge transfer separation, tunable light absorption, suitable band gap of 2.42 eV, and appropriate band alignment that makes it an efficient photocatalyst for solar fuel application [8]. However, despite the numerous advantages of CdS, it suffered from fast recombination and photocorrosion which hindered its productivity. The construction of heterostructure between CdS and other photocatalysts is considered the best way to enhance it photocatalytic performance [9]. S. liu et al. reported that CdS coupled with other cocatalysts such as TiO_2, ZnS, WO_3, etc., will be an effective technique to overcome the recombination effect of photo-induced charge carriers [10,11,12]. Recently, T. Kim et al. reported that rod-shaped CdS wrapped around WS_2 nanosheets under solar light produced a maximum hydrogen production rate of 3935.1 μmol h^{-1} g^{-1} with a quantum efficiency of up to 50% [13]. J. Bai et al. prepared CdS@Fe_2O_3-Ti_3C_2-$Zn_{0.7}$ Ohmic/S-scheme heterojunction and reported excellent hydrogen production of 8.93 mmol $h^{-1}g^{-1}$. It shows that using the cascade boundary of 2D connection in Ohmic S-scheme heterojunction reduced the lifetime of Zn-CdS, which is different from its average fluorescence lifetime. This reduction in lifetime potentially helps and prevent the recombination of photogenerated carriers, especially in CdS. However, it's noticed that their investigations on S-scheme charge transfer are limited particularly with n-n heterojunction [14]. Furthermore, X. Ning et al. prevented the photo-corrosion formed on CdS by adding a shell of Al_2O_3 and a TiO_2 film, resulting in a significant increase in H_2 production rate of 62.1 μmol h^{-1} g^{-1}, with a 6 and 126 times enhancement for the Pt/TiO_2@CdS and Pt-CdS@Al_2O_3 catalysts, respectively, when compared to CdS [15]. W. Zhen et al. reported that using Ni_2P@CdS or NiSe/MnO_2@CdS photocatalysts was successfully controlled and prevented the photo-corrosion of CdS throughs artificial gills that removed oxygen [16]. J. Zhang et al. reported that combination of CdS and g-C_3N_4 nanostructures exhibited significant photocatalytic activity under solar light [17]. X. L. Yin et al. prepared Ni_2P@CdS nano-heterostructure using green and in-situ synthesis and achieved exceptional H_2 production rate of 44.65 mmol g^{-1} h^{-1} [18]. Using hydrothermal method, Y. Wang et al. synthesized Mn-doped CdS@NH2-MIL-125 (Ti) nanocomposites. The results demonstrated a significantly improved catalytic activity, with an H_2 production rate of 3.61 mmol $h^{-1}g^{-1}$, compared to a single material [19]. R. Gao. et al. reported Pt/NFNi$(OH)_2$@CdS multi-heterostructured for H_2 production. The result shows H_2 production activity of ~ 44.05 mmol g^{-1} h^{-1}, this attributed to the reactivity of Ni ions with OH^- and form $Ni(OH)_2$ [20]. CdS-base photocatalysts can be modified into three strategies these includes the kinetics of surface reaction and separation of charges as well as stability as seen in Fig. 1 which demonstrated the modification strategies.

Therefore, adjustment of the co-catalyst, doping, and synthesis method is considered the best approach in solving the problem of CdS as a photocatalyst and improving the separation of photo-generated holes and electrons for H_2 production [21]. Incorporating metal and non-metal oxides can significantly enhance the higher activity. Herein, a comprehensive review has been designed to detail the role of CdS-materials for efficient solar fuel H_2 generation and applications. Nevertheless, to the best of our knowledge, there is no review, detailing the CdS materials as the main catalysts to produce sufficient H_2 in the literature with the exception of co-catalyst.

2. Crystal structure of CdS

CdS is widely known for its exceptional photochemical characteristics and photocatalytic performance by visible light irradiation [22]. The CdS structures are made up of tetrahedrally coordinated Cd and S atoms, where the Cd atom is surrounded by four neighboring S atoms, and vice versa. In the cubic zinc blend structure, the CdS^4 tetrahedra are arranged with the (111) plane in parallel, which is a plane that cuts through the center of the cube and intersects the four corners of the cube at equal distances. This arrangement of tetrahedra gives rise to a cubic symmetry, with the Cd and S atoms occupying alternating positions in a face-centered cubic lattice. In contrast, the hexagonal wurtzite structure, and the CdS^4 tetrahedra are arranged to the (001) in a parallel plane, which is a plane that is perpendicular to the c-axis of the hexagonal lattice as shown in Table 1. This arrangement of tetrahedra gives rise to a hexagonal symmetry, with the Cd and S atoms occupying alternating positions in a hexagonal lattice Fig. 2**.** The different arrangements of the CdS^4 tetrahedra structures upsurge the differences in both physical and chemical properties of the materials, such as its electronic band structure, optical properties, etc.

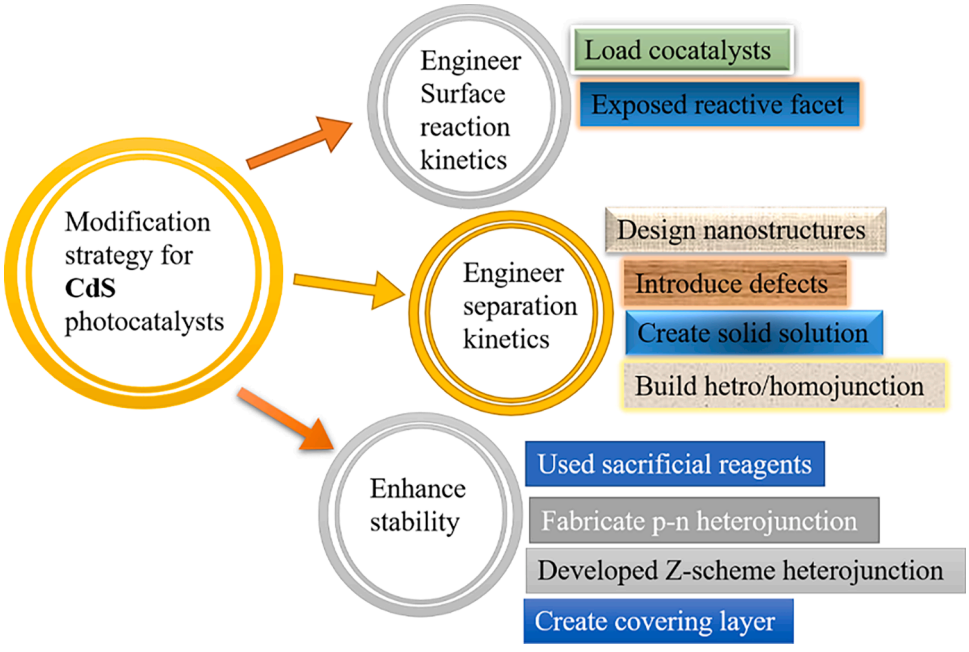

Fig. 1. Illustration of CdS base photocatalysts modification strategies.

Table 1
Displays information on CdS and its two crystal phases regarding their structural Parameters [24].

Structure type	Crystal phase	Space group	Lattice parameter	Atomic position
Wurtzite	Hexagonal	$P6_3mc$	$a = 0.4160$, $c = 0.656$	Cd(0.333, 0.667, 0), S (0.333, 0.667, 0.375)
Zinc blende	Cubic	$\bar{F}43m$	$a = 0.5832$	Cd(0, 0, 0), S(0.25, 0.25, 0.25)

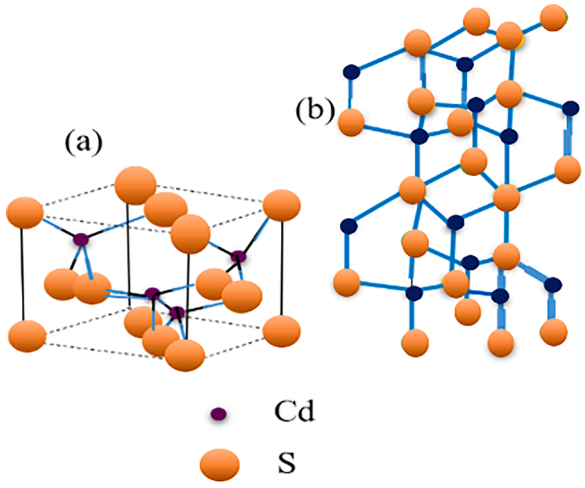

Fig. 2. Illustration of CdS crystal structures, (a) cubic-zinc-blend (b) hexagonal-wurtzite [23].

Generally, the synthesis of CdS at a temperature below 100 °C displays a cubic zinc blend phase. At higher temperatures usually above 300 °C there is the presence of a hexagonal wurtzite phase [25]. Higher crystallinity of CdS hexagonal phase is observed at ambient pressure and temperature and it's more stable than cubic phase. In line with many research works, the CdS hexagonal phase has a higher oxidation capacity for photocatalytic water splitting tests than that of the cubic phase usually for some common sacrificial agents e.g., sulfide (SO_3^{2-}) or (S^{2-}) [26].

3. Methods of synthesis of CdS photocatalyst

To overcome the crystalline structure, shapes, and dimensions, CdS is typically synthesized by different methods, namely, sonochemistry, solution-based approach, chemical bath deposition, solid state reaction, sol-gel method, solvothermal or hydrothermal etc.

3.1. Hydrothermal method

This method was introduced by Roderick Murchison a well-known geologist i.e., the term "hydrothermal" and later used for the synthesis of various nanostructures [27]. The technique involves preserving the precursor solution in a sealed chamber with high vapor pressure and temperature. The reaction undergoes several types of reactors such as bath reactors, autoclaves, and stirred reactors. Autoclave is commonly used because it is made of thick cylindrical wall steel containers with a cover that is airtight and can withstand high temperatures and pressure for extended periods of time. The temperature required for preparing photocatalysts may vary from 100 °C to 800 °C, and the pressure used is typically between a few bars to 2.5 Kbar [28]. However, synthesis via hydrothermal is typically undertaken below 300 °C; this is because of ionic products with maximum value between 250 °C and 300 °C respectively. At the supercritical state, the water solubility decreases resulting in the creation of ultra-fine nanoparticles [28]. The method has the following advantages (i) The precursors used are inexpensive (ii) The reaction is conducted under mild conditions (iii) The system is heated and pressurized to a point where the material becomes soluble and forms precise phases (iv) The materials obtained have high vapor pressure, low melting points, and are produced through pyrolysis (v) The final product's shape, size, and crystallinity can be precisely controlled by modifying parameters such as the solvent, surfactant type, reaction temperature, and precursor. Solvothermal synthesis results in a very high crystallization rate. The disadvantages include; (i) A high rate of aggregation (ii) Safety issues throughout the reaction are a concern (iii) Combustion may cause a significant risk of chemical contamination (iv) Expensive equipment is required for preparation (v) Mass production is challenging in solvothermal synthesis due to difficulties in controlling reaction conditions. Out of the methods mentioned, solvothermal synthesis has the advantage of controlling the nanocrystalline properties of histidine/CdS particles, resulting in an average size of 105 nm. This suggests that the crystallinity of the CdS nano-composite could be further improved. On the other hand, large particle sizes of 1.5 μm are commonly observed in the hydrothermal synthesis of histidine/CdS, which may lead to the reduction of specific surface area and poorer photocatalytic performance [29]. To put it differently, the size of CdS crystals can also be regulated through a method that involves solution. By doing so, it is possible to obtain CdS-based photocatalysts with fewer flaws. This approach can also lead to better distribution, ideal crystal structure, and reduced thermal strain [30]. Initially, CdS was created using a one-step hydrothermal method with a 1:1 CdS molar ratio. 0.925 g of $Cd(NO_3)_2{\cdot}4H_2O$ and 0.721 g of $Na_2S{\cdot}9H_2O$ were mixed in 20 mL of ammonium chloride solution at varying concentration levels between 1% to 9%. The resulting mixture was stirred for 15 min and then transferred to a Teflon-lined autoclave and heated at temperatures ranging from 160 °C to 220 °C for 24 h, as shown in Fig. 3. After cooling, the resulting material was dried at 80 °C for 24 h after cleansing with deionized water and ethanol [31].

3.2. Solid state reaction technique

In the past, CdS nano compounds were produced through solid and liquid phase synthesis techniques, where the method used, raw materials, reaction time, and temperature affected the morphology and crystal phase. The solid-state reaction method took place at the interface of the phase, resulting in granular morphology with low crystallinity and

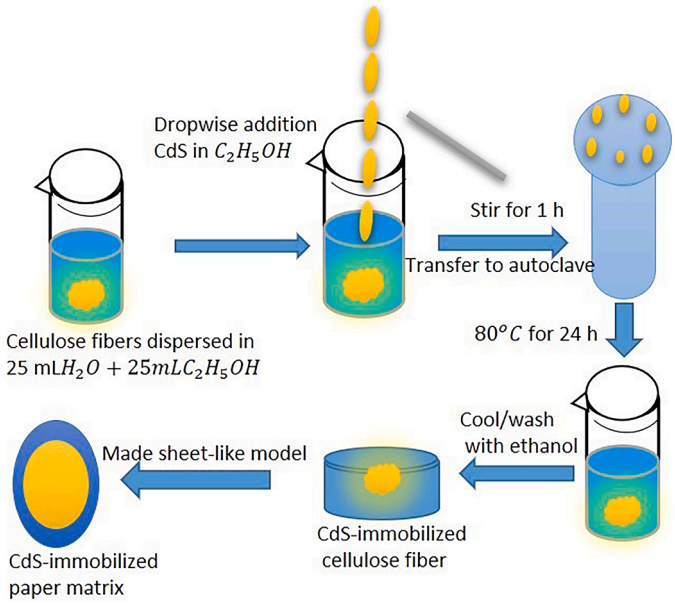

Fig. 3. Schematic of hydrothermal synthesis for CdS [32].

high energy consumption.

Solid-state reactions involve solid mixtures that do not react at normal room temperature. When an external force is applied, the particles of the reactant and the reacted powder come together, resulting in what is known as a mechanochemical reaction [33]. When subjected to higher temperatures, the substance produces an end result and its atoms disperse throughout the material's interior through a process called diffusion. This leads to the occurrence of nucleation processes as the temperature increases. The sole phase in which all components are combined at the atomic level is the solid solution [34]. It is true that the properties and structure of a material can change as its constituents change. Solid-state reactions can often lead to the formation of materials with different properties than their individual components. In addition, the crystal structure of a material can also changes during solid-state reactions, leading to changes in properties such as density, strength, and thermal conductivity. Solid-State reaction technique has the following advantages and disadvantages; the advantages are: (i) easy fabrication, (ii) simple to scale up, (iii) the process is low cost [35]. The disadvantages include [36]: (i) the grain morphology is usually found to be non-uniform, (ii) inconsistency (iii) lack of purity because the formation of the product does not occur at the ionic level etc.

3.3. Sol-gel method

Sol-gel method was first introduced by Ebelman (1845) [37]. The process involves three steps: sol preparation, sol gelation, and solvent removal. The sol is a colloidal suspension obtained from a solution of inorganic liquids such as metal chlorides and alkoxides. The sol particles are mono-sized nanoparticles that are held together by surface charges and Van der Waals forces, which create a Columbic repulsive force. The sol suspension contains amorphous materials ranging from 1 nm to 1 μm in size. The gel is a highly viscous material that forms when the solvent begins to evaporate, creating a solid solvent-encapsulating matrix. During the evaporation process, the sol particles connect thereby forming a network of gel-like particles. The sol is made by incomplete condensation and/or hydrolysis of inorganic salts and/or alkoxides, which creates metal-oxo-metal or meta-hydroxy-metal bonds for gel formation. The time taken for the transformation of the liquid solution is known as the time for gelation, which may take a few minutes or hours. An increase in time results in shrinkage of the solution and solvent expulsion. Aerogel and xerogel formation occur when the gel is dried at supercritical conditions or ambient pressure. The mechanical properties of nano-sized particles are improved by calcination processes, which remove metal hydroxide groups at high temperatures close to 800 °C, resulting in shrinkage of the particle's surface area [38].

The sol-gel process is affected by various parameters such as reaction time, temperature, type of solvent, precursor, pH of solution, concentration of precursor as well as the solvent. There are two types of sol-gel methods: aqueous and non-aqueous. In the aqueous method, water is the solvent while alcohol is used in the non-aqueous method. Amorphous precipitates are more commonly formed in aqueous solutions, which is a disadvantage compared to the non-aqueous route. Despite this drawback, sol-gel is still utilized to prepare Wurtzite (hexagonal phase) or sphalerite (cubic phase) cadmium sulfide [39]. Sol-gel has several benefits compared to other techniques, including its ability to regulate porosity and particle size while maintaining high purity. It is also cost-effective and enables the creation of nanoscale materials at low temperatures. However, one significant drawback is that some of the organic solvents employed may be hazardous, and the processing time may be lengthy [40]. The sol-gel method is used to introduce metal-positive ions into the crystal lattice of CdS through doping. Typically, this involves substituting or inserting transition metal positive ions such as Zn^{2+}, Mn^{2+}, Ni^{2+}, etc. in place of Cd^{2+} ions, with similar ionic radii and charges to Cd^{2+} (which has an ionic radius of 0.85 Å). This process can improve the stability and photoactivity of the doped CdS, making it more effective for hydrogen production [41]. The method has the following merits and demerits; the merits of using the sol-gel method include (i) low-temperature synthesis, (ii) a greater ability to manipulate the shape, structure, and size of particles, and (iii) the potential to control the purity of the final products by carefully selecting the initial precursor. Hence the disadvantage is that the solitary challenge with the sol-gel technique is the extended time required for the creation of the precipitate.

3.4. Co-precipitation method

The co-precipitation approach is similar to the precipitation method, as both rely on super-saturation conditions to produce insoluble products. In the formation of a photocatalyst via co-precipitation, several crucial steps occur, including nucleation, growth, coarsening, and agglomeration. The creation of a homogeneous precipitate through the mixing of two or more salt solutions is dependent on differences in solubility and precipitation kinetics. Precipitation kinetics involve nucleation as well as growth of the precipitated particles, this situation is governed by various factors. The pH level, level of supersaturation of the solute, and other similar factors can strongly influence various processes [42]. The advantages and disadvantages of the co-precipitation method are; its simplicity and speed of preparation, the ability to control particle size and composition with ease, and the relatively low temperatures required for the process. Additionally, there are various options available to regulate particle surface state uniformity, and the process does not involve the use of organic solvents. The disadvantages are; that it's time-consuming, issues with reproductivity, and the potential for impurities to precipitate with the final products. Additionally, co-precipitation may not be effective if the initial reacting species possess a distinct precipitation rate. Proper monitoring of the entire process is crucial to ensure that the pH of the solution is adjusted as needed, leading to high-quality products.

Comparably to the precipitation method, co-precipitation is viable in the condition of super-saturation where the resulting nanomaterials are insoluble. The process of producing nanoparticles of Cadmium Sulfide involved adding solutions of cadmium in 500 mL of distilled water, and then slowly adding a solution of sodium sulfide drop by drop while stirring. The resulting solution was left to stir for an hour, which caused a yellow and white precipitate to form for the cadmium sulfide solution. After 24 h, the stirring was stopped, and the particles were washed with isopropyl alcohol and water to prevent them from clumping together. The particles were then allowed to settle, and dried in an oven at 90 °C for 12 h. The same process was used to prepare nanoparticles of CdS [43].

4. Photocorrosion mechanisms of CdS

The photocorrosion of pristine CdS is primarily ascribed to the oxidation of surface lattice sulfur through its photogenerated holes. As a result of high photoinduced holes on the surface of the sulfide, the sulfide will become greatly unstable as a photocatalyst [44]. Generation of electrons as well as holes will occur when the metal sulfide is irradiated for appropriate light irradiation. In this regard, the excited electrons in a photo-sensitive material will move to the surface without any difficulty. Later on, the photogenerated holes will gather on the outermost surface of the sulfide and subsequently be used by the donors of electrons present in the reaction system [45]. Therefore, Sulphur or sulfate oxidation might occur, and the working properties of the material in the photocatalytic reaction are inhibited hence resulting in the oxidation of photocatalyst [46,47]. Photocorrosion is important for the oxidation of photo-induced holes within a semiconductor and can be minimized by inhibition of a newly formed oxygen within the water [48]. On considering H_2 and O_2, in water O_2 is higher soluble, therefore O_2 has the highest tendency to cause photocorrosion of CdS in the photocatalytic H_2 production. The photocorrosion of CdS would be accelerated if the oxygen combined with the induced light-electron creates O_2

radicals [48]. The cause of photocorrosion by two-hole leading to oxidation reaction can be seen in eqn. (1).

$$CdS \rightarrow e^- + h^+ \quad (1)$$

$$CdS + 2h^+ \rightarrow Cd^{2+} + S \quad (2)$$

Thus, eqn. (3) and 4 represent the presence of oxygen which account for CdS photocorrosion.

$$CdS + 4h^+ 2H_2O + O_2 \rightarrow Cd^{2+} + SO_4^{2-} + 4H^+ \quad (3)$$

$$O_2 + 4e^- + 2H^+ \rightarrow 2OH^- \quad (4)$$

$$CdS + 2O_2 \rightarrow Cd^{2+} + SO_4^{2-} \quad (5)$$

4.1. Eliminating oxygen from the photocatalytic system

It is well known that CdS is a potential candidate in photocatalytic H_2 production which shows excellent activity for water splitting in the presence of sacrificial reagents e.g., Na_2S/Na_2SO_3, lactic acid, ethanol, etc. Hence, it is desirable for practical application to construct an overall based-CdS photocatalyst for a water-splitting system. The main considerable factor of the caused photocorrosion of CdS-based photocatalysts is photogenerated holes. However, for the water-splitting process, the nascent oxygen impact on semiconductor stability is disregarded. Despite the fact that in water oxygen solubility is greater than H_2 [49]. High oxygen solubility has a negative effect on the CdS photocatalyst, causing an increased serious photocorrosion in CdS. However, reverse recombination of oxygen and H_2 is caused by excess oxygen accumulation in water, this is due to the fact that low energy activation (16.5 kJ/mol) of oxygen and H_2 recombination regardless of whether there is light irradiation or not, over co-catalyst, hinders the effectiveness of water splitting for a semiconductor. Thus, it has become mandatory to eliminate oxygen from photocatalytic water splitting via some reagent for better stability and to enhance the efficiency of H_2 production using CdS-based photocatalysts [23].

The effect of photocorrosion of CdS-based photocatalysts can be overcome by using many strategies to improve its stability, this might be achieved by; i) Perfluoro decalin (PFDL), is a completely fluorinated organic compound stands as an exceptional synthetic oxygen carrier, possessing high oxygen blend capacity. ii) TiO_2 anti-photo corrosion layer, semiconductors with wide bandgap have been considered a promising candidate for enhancing the stability of sulfide photocatalytic systems. iii) Al_2O_3 anti-photo corrosion layer, a stable metal with chemical inertness has been regarded as a catalytic supporter. Other semiconductors that act as an anti-photocorrosion layer and also can serve as coating materials include; NiO, WO_3, MnO_2, Cr_2O_3, Ni_2P, and artificial gill respectively [50].

5. Photocatalysts for hydrogen production

Photocatalysis received significant attention in research as a viable method for converting solar energy through the surface of photocatalyst, which has the potential for hydrogen production and water splitting. Due to the fast-growing demand for photocatalysts for H_2 production, one crucial contest in this process is the design of visible light active, inexpensive materials, and methods for H_2 production. Hence, designing an appropriate catalytic structure that can significantly upsurge the gain in photon ability, and improve reduction efficiency that can lead to intrinsic catalytic ability toward H_2 production is required. There are many procedures for photocatalytic H_2 production such as migration, generation, and separation of photogenerated carriers, light absorption by virtue of photocatalysts, and generation of H_2 and O via free electrons and hole's reaction with H_2O respectively. Therefore, many nanocomposites and nanostructures of inorganic semiconductors are efficient for photocatalysts growth such as metal oxides (ZnO, TiO_2, Cu_2O, V_2O_5, WO_3, MoO_3, ZrO_2, CoO, etc.), metal sulfides (MoS, CdS, $ZnIn_2S_4$, ZnS, $CuInS_2$, etc.), metal selenides (ZnSe and CdSe), oxynitrides ($LaTaON_2$, TaON, and $BaTaO_2N$), and organic semiconductors which includes g-C_3N_4 are widely used for photocatalytic H_2 production [51]. In photocatalytic reactions, some possible mechanisms need to be considered including heterogeneous and homogeneous photolysis.

5.1. Photocatalysis for water splitting

The fundamental of photocatalytic water splitting is considered artificial photocatalysis since it looks like a process of photosynthesis in green plants below solar energy. The H_2 production from water/wastewater could be succeeded via photocatalytic processes through the advantage of sun radiation that always invades the earth's surface [52]. During the photocatalytic process, there is noticed energy conversion in light energy which is converted to chemical energy, as such Gibbs free energy is built up by water splitting reaction [53]. Two techniques are considered to produce H_2 such as the photocatalytic water splitting and photocatalytic reforming of organics [54]. In the initial technique, with electron holes, water endures a redox reaction, while in the other technique, the donated electron by an organic substance oxidizes to generate proton ions which are finally converted to H_2 through the electron participation over the photocatalyst [54].

When chemicals are reacted in the presence of a suitable photocatalyst, which absorbs visible, ultraviolet, or IR light, the process is known as a photocatalytic reaction [55]. Such reactions involve several crucial stages, starting with light harvesting, where a photon with appropriate energy triggers the photocatalyst. The following step involves the stimulation of electrical charge, whereby electrons from the valence band (VB) are stimulated to move to the conduction band (CD), resulting in the formation of photoexcited electrons and holes in both the conduction and VB of the photocatalyst. The primary challenge in photocatalytic water splitting is the speed at which the photogenerated electrons and holes recombine [56]. The photoexcited electrons and holes serve as forceful oxidizing and reducing agents, driving oxidation–reduction reactions. However, the process of recombination, which can occur through radiative or non-radiative transitions, hinders the movement of photoexcited electrons from the conduction to the valence band. This leads to the loss of electron-hole pairs. To overcome this, any remaining free electrons or holes diffuse to high-energy locations on the surface. In water oxidation is causing by photoexcited holes transport, creating protons (H^+), while the photoexcited electrons are participated in (H^+) reduction creating molecular hydrogen [57]. The performance of CdS in photocatalytic processes is heavily influenced by its band structure. In CdS, the S^3p orbitals contribute to the highest point of the VB, while the Cd^5S and 5p orbitals contribute to the lowest point of the CB. Typically, the dissociation of water for water splitting requires high temperature exceeding 2070 K. However, this reaction can be achieved at room temperature through the use of photocatalyst under the influence of light with energy [58].

$$catalyst \rightarrow catalyst\ (e^+ + h^+) \quad (6)$$

$$catalyst\ (e^- + h^+) \rightarrow catalyst \quad (7)$$

$$H_2O + h^+ \rightarrow \frac{1}{2}O_2 + 2H^+ \quad (8)$$

$$2e^- + 2H^+ \rightarrow H_2 \quad (9)$$

$$RCH_2OH + 2h^+ \rightarrow RCHO + 2H^+ \quad (10)$$

The main challenge associated with photocatalytic water splitting is the tendency for the photogenerated electrons and holes to recombine, which results in the release of unproductive heat, as shown in Eq. (7). Therefore, when studying photocatalysis for water splitting, sacrificial agents like Triethanolamine (TEOA), lactic acid, ethanol, methanol, and

electrolytes such as Na_2S/Na_2SO_3 etc., are important to prevent the recombination [59]. In general, electrolytes do not undergo reduction or oxidation through the CB and VB of electrons/holes. Instead, they have the capability to move ions and facilitate electron transfer to nearby semiconductors, which can enhance the process of photocatalytic water splitting.

To achieve efficient photocatalysis, it's necessary for the energy difference between the electrons (e^-) and holes (h^+) to be greater than the required energy for the targeted redox reaction, and for the redox reaction rate to be faster than the rate of e^-/h^+ recombination Fig 4. Generally, photocatalysis involves five key processes: light absorption, excitation, charge separation, transport of charge carriers, and surface reactions on the catalyst. However, if the bandgap energy is low, there's a risk of competing process, charge carrier recombination which is seen as a significant drawback of photocatalysis.

6. Oxygen evolution reaction (OER)

The oxidation of hydroxide ions or water molecules into oxygen molecules on the anode surface is known as the oxygen evolution reaction (OER). In the characteristic of water splitting OER is critical due to its inactive kinetic. This is the reason why OER catalysts always exhibit a high overpotential of 300 – 400 mV. Therefore additional work is required to overcome overpotential [61]. Oxygen evolution reaction has four electron oxidation reactions comprising *OH, *O, and *OOH intermediates. Owing to the presence of an acidic medium water molecules oxidize when electrons produce an OH group and the proton then adsorbs on the catalyst surface (OH*ads). An additional oxidation of OH*ads ejects the proton and a surface-adsorbed oxygen atom (O*ads) remains. At this point, the reaction pathways can proceed along two distinct routes. Water molecules react with the low concentration of O*ads to produce OOH*ads group in the first place in the presence of OOH*ads group hindered by oxidation there is exist oxygen molecules. This may occur if the surface of the catalyst is highly occupied by O*ads, the neighboring O*ads atoms can undergo a reaction with each other, resulting in the formation of oxygen molecules. In the case of an alkaline medium, OER is somewhat different from that of an acidic medium. Instead of the water molecule, the abundant hydroxide ion experiences single-electron oxidation on the catalyst's surface, producing a proton and an adsorbed hydroxyl radical (OH*ads) [62]. The second oxidation stage is when hydroxide ion reacts with OH*ads and the primary steps for O*ads and water molecules. A high concentration of O*ads results in the formation of oxygen molecules. In contrast, the O*ads interact with the hydroxide ions, leading to a two-step oxidation process through the intermediate formation of the OOH*ads group. This eventually results in the production of oxygen molecules and a molecule of water. The formation of OH*ads and OOH*ads groups plays a vital role in the OER. Similar to the HER, the change in Gibbs free energy of O*ads ($\Delta G_O{}^*{}_{ads}$) is a critical parameter used to assess the OER activity of a specific electrocatalyst. The pH solution has a direct influence on the OER. For example, in alkaline conditions, water undergoes disassociation into oxygen and protons, while hydroxyl ions are oxidized to produce oxygen and water [62].

7. Hydrogen evolution reaction (HER)

The phenomenon that occurs at the side of the cathode which brings a decrease of protons or water molecules into molecular hydrogen is known as the hydrogen evolution reaction (HER) [63]. The HER is significant in the electrochemical process with a critical role in water splitting, the reaction occurs in the cathode, and the mechanism as well as the kinetic are frequently explored. Under a critical electrolytic cell, the key components of electrocatalytic water splitting basically utilize the anode, cathode, and electrolyte for neutral, alkaline, or acidic, water. Over potential dropping and increasing the efficiency of the electrolysis is dependent on the electrocatalyst [64]. The cathode is the

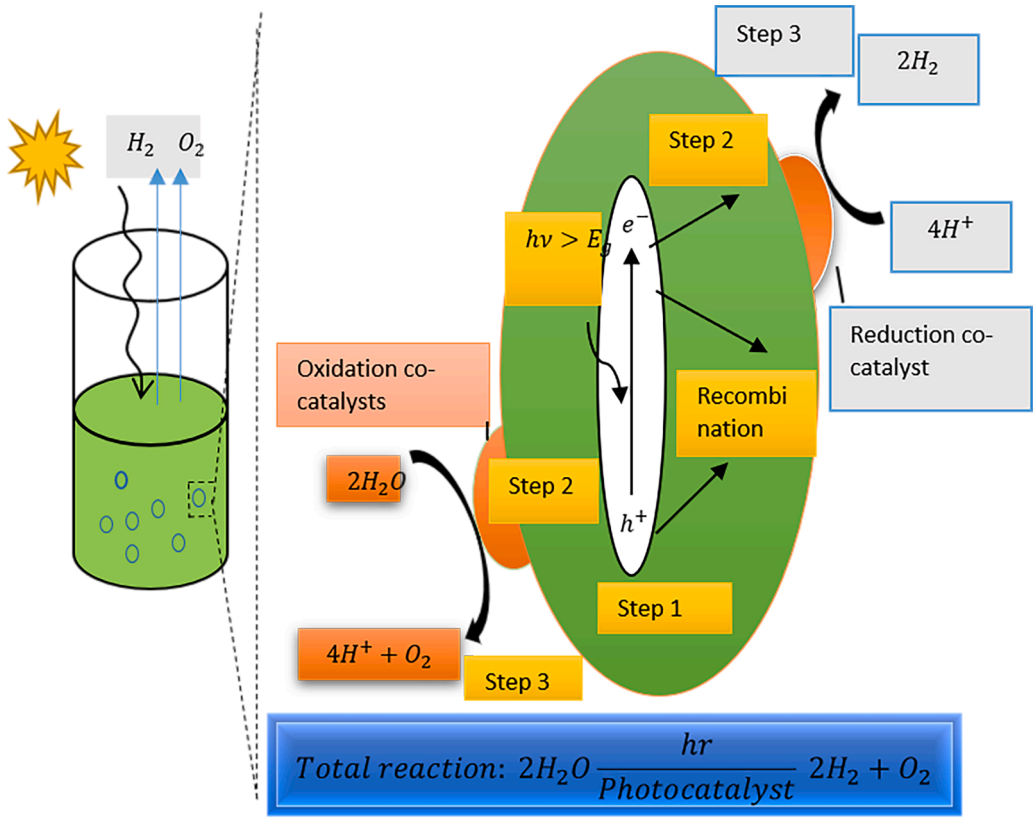

Fig. 4. Schematic overall photocatalytic water splitting for light irradiation [60].

initial process and single electron proton reduction, subsequently, the adoption over the cathode surface is called the 'Volmer reaction' Eq. (6) below. Two steps are well recognized for hydrogen molecule formation these are well determined from the number of adsorbed hydrogen atoms (H^*ads). If the H^*ads concentration is much lower, H^*ads atom is needed for hydrogen molecular formation to obtained the desired proton as well as the electron from the solution, Eq. (7) below and is called Heyrovsky reaction. Furthermore, if H^*ads is high, the molecule of hydrogen evolution would occur via a combination of two adjacent H^*ads atoms on the surface of the cathode which satisfied Eq. (8), and is called Tafel reaction [63]. Hence the exist three equations for elemental reactions proposed for HER in acidic media includes:

$$H^+ + {}^* + e^- \underset{\rightarrow}{\overset{\leftarrow}{}} H_{ads} \ (Volmer\ reaction) \tag{6}$$

$$H^+ \ + \ H_{ads} + e^- \underset{\rightarrow}{\overset{\leftarrow}{}} H_2 + {}^* (Heyrovsky\ reaction) \tag{7}$$

$$2H_{ads} \underset{\rightarrow}{\overset{\leftarrow}{}} H_2 \ (Tafel\ reaction) \tag{8}$$

From the equation, this means (*) the active site of the catalysts surfaces the intermediate surface can adsorb. Furthermore, hydrogen production from water splitting through hydrogen evolution is a result of renewable resources, which is in line with future sustainable energy supply, as such there is a need for adequate photocatalysts to recover the efficiency of the energy conversion [63]. However, one of the significant parameters to estimate the target electrocatalysts for efficient water splitting, the electrocatalysts should have low overpotential to attain 10 mA cm^{-2} (η_{10}). Hydrogen evolution reaction should display a proper H^*ads which is an indication that the Gibbs free energy change of H^*ads (ΔG_{H^*}) would be nearly to zero [63]. The binary metal atom catalysts with a unique advantage for spinning H^*ads because of the special coordination structure [65]. Hydrogen evolution reaction super with many challenges for instance, on the surface of electrocatalysts hydrogen bubbles may adhere and block the active sites, upsurge overpotential, and generate unwanted electrolyte diffusion, consequently, worsening the HER performance [66]. Enhancing the performance of electrocatalysts for the HER poses additional challenges, such as enhancing the atomic utilization of Pt and developing noble-metals electrocatalysts with increased intrinsic activity. Again, there is a need for an upsurge in catalytic active site density to attain the desired current density by reducing the overpotential. However, enhancing the catalyst conductivity is an advantage for lessening the ohmic resistance for electron transfer to be efficient. Currently, in industrial settings, alkaline electrolytes are employed for the electrocatalytic HER due to the detrimental effects of equipment corrosion and the potential contamination of acidic electrolytes with acid steam [61].

To enable the efficient and cost-effective mass production of hydrogen using the electrolytic HER, it is crucial to obtain electrocatalysts that possess the following characteristics: excellent conductivity, a substantial quantity of active sites, effective formation of gas bubbles, capability to generate high levels of electrical current, affordable synthesis costs for large-scale manufacturing, stability in both acidic and alkaline conditions, and availability of abundant earth-based materials.

7.1. Photoelectrochemical for hydrogen generation

Hydrogen is produced from water in photoelectrochemical water splitting by the use of sunlight and semiconductors known as photoelectrochemical materials, whereas irradiated light energy dissociates molecules of the water into H_2 or O_2. The key components of photoelectrochemical cell (PEC) water-splitting semiconductors are light-absorbing photoelectrodes, electrolytes, and separation of membrane. In terms of sustainable H_2 generation PEC has numerous advantages e.g., it is appropriate for portable and stationary applications, pressures and temperatures are moderate to operate, etc. The photoelectrochemical system is similar to the one used in photovoltaic solar production; sunlight is applied to activate water-splitting by putting the semiconductors in water-based electrolytes in a photoelectrochemical application. Electrons moved up to the higher energy level when the electrode of the semiconductor absorbed light, at the same time electrons and holes at the liquid interface, may undertake redox reaction processes. In photoelectrochemical water splitting the procedure involves energy conversion in which light energy is converted to chemical energy. The transport of electrons and hole pairs is prevented through massive amounts of photogenerated carriers. By incorporation of Nb with CdS will promote adequate transmission of photogenerated charges indicating that a successful PEC can be achieved by enhancing the division of electron and hole pairs [67]. The advantages of photo-electrochemical are; that it is economically feasible and convenient for synthesis and processing, easy to manufacture, possibility of in situ storage. Considering the advantage of using direct sunlight, PEC schemes are environmentally benign, chief, and efficient ways to produce H_2 respectively. CB and VB are the main parameters to be considered in water splitting as mentioned earlier. In PEC water splitting the conduction band of the selected semiconductors must have a higher energy band over the reduction potential and lower valence band energy than the oxidation potential with a band gap of about 2 eV respectively [67].

8. General mechanism of photocatalysis

Efficient water splitting in photocatalytic H_2 production requires a suitable band gap of greater than +1.23 eV. Both the CB and the VB play important roles in proton reduction reactions and H_2O oxidation in semiconductors. The material band gap must allow a wide spectrum for effective solar radiation absorption. Additionally, the photoelectrodes must have effective charge transport under various operating conditions. The surface band-edge position of the semiconductors provides the highest oxidation–reduction possibilities for photogenerated electrons and holes. Therefore, semiconductors with a narrow bandgap (~1.23 eV) are considered a potential candidate for photocatalysts in water splitting. In photocatalytic H_2 production, overpotential and reorganization energies are caused by the process of interfacial charge transfer, and this increases the lowest potential requirement for the photocatalytic H_2 production process and lessens the solar to H_2 efficiency almost by 18% [68].

The mechanism of photocatalytic water splitting can be divided into several phases. Firstly, when the semiconductor absorbs energy that exceeds its band gap, it generates pairs of electrons and holes. Secondly, according to Eq. (9), water is oxidized by these holes (h^+) to create both H^+ and O_2. Thirdly, the photogenerated electrons (e^-) migrate to the CB and generate H_2 by reducing H^+ ions, as shown in Eq. (10). Finally, Eq. (11) also plays a role in this process. In photocatalytic water splitting knowing these concepts is significant. These include Planck's constant (h), light frequency (n), band gap energy (E_g), VB, and CB. In addition, understanding the catalyst and sacrificial donor is essential. Once the catalyst absorbs sufficient light, it can initiate the processes of H_2 and O_2 evolution by breaking down water which can lead to water splitting [69]. By introducing a sacrificial donor, the vacancies that lead to self-oxidation are eliminated, resulting in a decrease in charge carrier recombination. This, in turn, enhances the production of H_2 and O_2. Generally, water splitting involves the following reactions [69].

$$H_2O + 2h^+ \rightarrow 2h^+ + \ 1/2O_2 E^o oxidation = -1.23\ V \tag{9}$$

$$2H^+ + 2e^- \rightarrow H_2 E^o oxidation = 0.00V (2) \tag{10}$$

$$Overall\ reaction: \ H_2O \rightarrow H_2 + 1/2O_2 \tag{11}$$

A suitable band gap less than 1.23 eV is required for photochemical water splitting; and required a least thermodynamic potential around

1.23 eV.

8.1. Heterogeneous photocatalysts

One of the types of photocatalysis that produces chemical reactions is heterogeneous photocatalysis, the transformation here is that catalyst and light are well required. At the surface of the heterogeneous semiconductor, the reactivity of a large scope of adsorbates is impacted, and redox reactions are induced in these molecules by light emission from the surface. By introducing light, there would be a generation of highly explosive species, which are holes (h^+), superoxide ions ($O_2^{\bullet}$), hydroxyl radicals ($OH^{\bullet}$), and peroxide radicals ($HO_2^{\bullet}$) [70]. The formation of contact between the hard metal photocatalyst, the reaction of the product, and the conditions for liquid reaction holding is entailed by a heterogeneous photocatalysis scheme [70]. Usually, heterojunctions (type II, type II, type III), Z-scheme heterojunctions, p-n heterojunctions, and S-scheme, etc., are considered heterojunctions that can be categorized on their structural types [70].

8.1.1. Type-I heterojunctions

In this type of heterojunction photocatalyst, photons generating e^-/h^+ that easier to move from the CB of semiconductor with high energy level to other semiconductors Fig. 5. Owing to the inability to separate carrier charges of the type-I heterojunction which resulted in the accumulation of e^-/h^+ at the same semiconductor which cause rapid recombination. At the same time, the processes of photocatalysis in semiconductors are observed with low reduction and oxidation potential, as such the photocatalysis efficiency decreases under visible light irradiation [71].

8.1.2. Type-II heterojunctions

The alignment of band gaps can be attained by creating a high-quality heterojunction between CdS and certain other semiconductors, which offers an alternative approach to manipulate the charge separation kinetics of CdS [73]. Type II is the most effective method for separating electron-hole pairs, and noble metals are commonly used to create heterojunctions as shown in Fig 6. In type II heterojunctions' electrons are migrating in semiconductors at a lower level of conduction. Concurrently, within the device holes are moving with a high VB level, diminishing the interaction between e^-/h^+ interaction and recombination [74]. For example, Yang et al. produced CdS/ZnO core/shell nanofibers using a type-II heterojunction and discovered that they had better photocatalytic activity for H_2 production than CdS or ZnO alone. Graphene is another promising material for creating heterojunctions with CdS, as it has good electron conductivity and a suitable potential of (−0.08 V, pH = 0). When CdS generates photogenerated electrons, they tend to flow onto the surface of graphene, promoting efficient separation

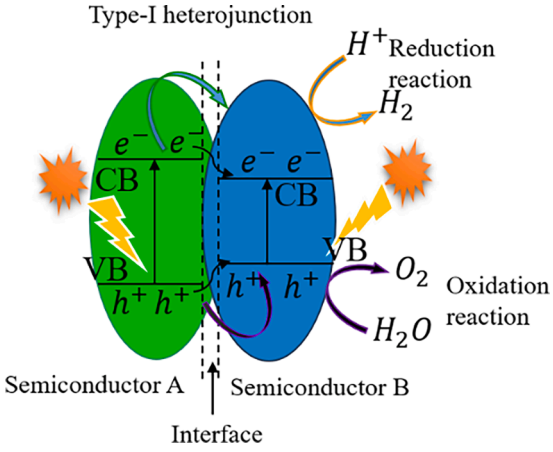

Fig. 5. Illustration of type-I heterojunction photocatalysts [72].

of electron-hole pairs [75].

However, despite the similarities in structure between type-III and type-II heterojunction formations, there is a significant difference in the energy bandgap at the interface due to the elevated energy levels within the band.

8.1.3. Evolving heterojunction for Z-scheme charge transfer mechanism

Owing to the different mechanisms of photocatalysis, Z-scheme is also another type of mechanism describing the photogenerated electrons transfer between the photocatalysts. The light illuminated photogenerated electron-hole pairs of two semiconductors (S1 and S2) [76]. The effectiveness of solar energy utilization with photocatalytic semiconductor materials primarily relies on their characteristic band-gap energy (Eb_g), which is determined by the CB and VB sites of S1 and S2, the exciting electrons to the CB requires sufficient energy [77]. The capability of oxidation and reduction of photo-generated e^-/h^+ pairs are determined by the band positions. When the position of the conduction band is negative and the position of the valence band is positive with respect to the balanced potentials, photo-induced e^-/h^+ pairs can effectively participate in surface oxidation and reduction reactions [77]. The oxidation and reduction photocatalysts possess low valence band in position with strong oxidizing properties, the subsequent one is reduction photocatalysts which have higher conduction band positions and effective reduction abilities that usually occurs in hydrogen production [78]. A. J. Bard et al. (1979) proposed that Z-scheme photocatalysts have the potential to overcome the reduction in the oxidation–reduction ability of photocatalysts that occurs due to electron-hole separation and this finding was found to have many problems. This is because Z-scheme photocatalysts can maximize the oxidation–reduction potential of heterojunction [79]. The successful creation of a photocatalyst with a solid-state Z-scheme was achieved using two semiconductors, MnO_2 and CdS, as an intermediary, Au, to enhance the photocatalytic production of H_2. The movement of photogenerated electrons from the VB to CB of MnO_2 and then to CdS VB through the Au intermediary is considered to be the cause of the improvement. The band alignment of these phases creates a type-II junction, allowing for the suppression of charge recombination by the migration of charges within the internal and external charge space regions. However, the CB site of CdS is negative compared to MnO_2, while the VB site of MnO_2 is positive compared to CdS Fig. 6. Therefore, the Z-scheme charge transfer mechanism is more effective in photoreduction of photogenerated electrons, but not only ineffective separation of photogenerated charges, than the conventional charge transfer mechanism [80]. Despite numerous studies that have extensively discussed four basic primary photocatalytic mechanisms are considered: (i) separation of photo-induced charge carriers; (ii) surface oxidation–reduction reactions induced by photo-generated electrons and holes; (iii) transport and movement of charge carriers to the active oxidation–reduction sites on the surface of the photocatalyst; and (iv) light absorption by the photocatalyst [81]. To overwhelm the effect of photo corrosion (S^{2-} oxidation), and enlarge the light absorption, developing advanced CdS nanostructure is an important strategy for the efficient separation of photogenerated e^-/h^+ pairs [82].

The process shown in Fig. 7 involves the accumulation of photoinduced electrons in CdS and holes in MnO_2 through the electron-transfer system Au (represented by a black narrow arrow). The accumulation of these charge carriers is physically separated, with the CdS surface reducing and MnO_2 surface oxidizing (represented by a white wide arrow) in different locations. However, these two functions combine vectorially to create a continuous driving force for the photoinduced charge carriers. The electrons are concentrated in the conduction band of CdS, while the holes remain in the valence band of MnO_2. Yet, all the mechanisms discussed encounter several difficulties during their fabrication and are regarded as wrong. If water-free electrons cannot exist, then the photogenerated electrons can never transfer through a water medium, hence the Z-scheme charge transfer mechanism is inappropriate. The composite reduction ability decreases with the transfer of

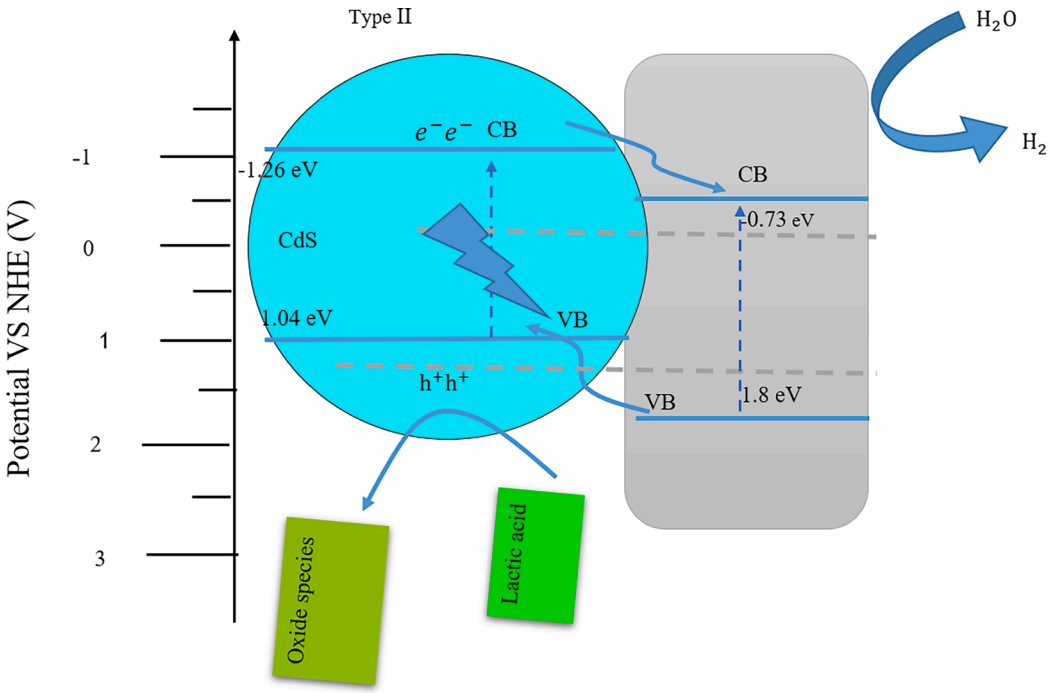

Fig. 6. Schematic representation of type-II heterojunction.

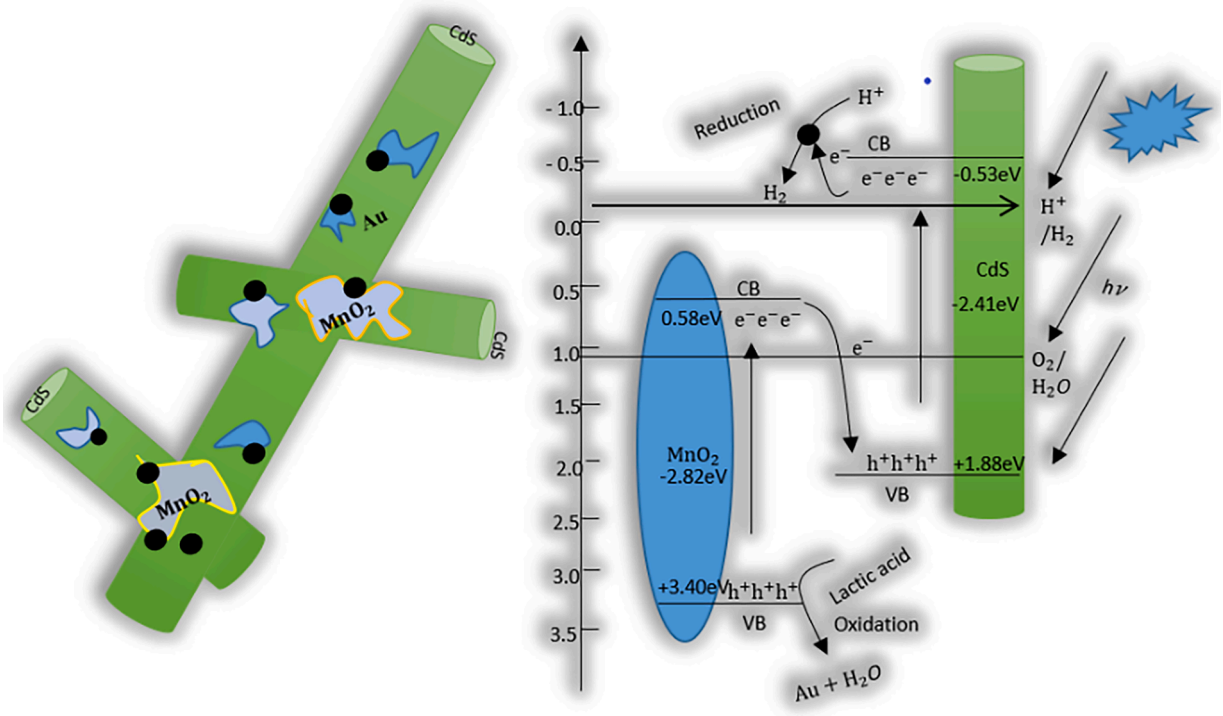

Fig. 7. Illustration of charge transfer and H_2 production of the Z-scheme photocatalyst CdS@MnO_2/Au.

photogenerated electrons from high to CB. However, this transfer occurs with the holes from low high VB, which lowers the oxidation ability. Again, electrons are difficult to transfer from the CB of two different photocatalysts due to strong electron-electron repulsion [72]. Likewise, holes are difficult to transfer from low to high VB. Finally, its diminutions the energy of photogenerated electrons and holes. Hence, the mechanism of carrier transfer of type II heterojunction is wrong [76]. J. Yu and his core workers reported in 2019 and 2020, that the charge transfer mechanism of type-II, all solid-state Z-scheme, and liquid-phase heterojunctions were wrong [83,84]. These difficulties have prompted the creation of S-scheme heterojunctions which are now replacing Z-scheme.

8.1.4. Evolving heterojunction for S-scheme charge transfer mechanism

The construction of an S-scheme heterojunction will involve reduction photocatalyst (RP) and oxidation photocatalyst (OP) with staggered band structures, the direct Z-scheme heterojunctions lack strong redox ability, due to the limitation type-II heterojunction by charge transfer

mechanism from the kinetic point of view. The S-scheme heterojunction is derived from the Z-scheme which maintains an effective redox potential and enhances the recombination of unnecessary electron-hole pairs [85]. Meanwhile, the photogenerated hole has a negative impact which donates to oxidation photocatalysts, but the photogenerated electron has no impact [84]. Photogenerated electrons and holes accumulate upon the CB of the OP as well as the VB of the RP, resulting in type-II heterojunctions having a lower redox capacity [83].

Eventually, the CdS@MnO_2 junction composite is the collection of RP and OP here with opposite surface charges, and at the less defective junction, the unnecessary recombination of electron-hole occurs, hence accelerating electron transfer and improving charge separation. As a result of the oxidation reaction, an excellent photocatalytic H_2 product is achieved. It is therefore inferred that CdS@MnO_2 heterojunction follows the S-scheme charge transfer mechanism, Spin-trapping ESR analysis was performed to detect •OH and •O_2-in H_2O_2 and methanol solutions by using DMPO as a free-radical trapping agent to estimate the S-scheme charge transfer path in CdS@MnO_2 junction. Fig. 8, represents the mechanism for H_2 production in the CdS@MnO_2 catalysts. The electron in the conduction band of CdS excited by a single source of light corresponding to the wavelength transferred to the conduction band which migrates to the valance band of MnO_2 and recombined with the holes.

The built-in electric field is produced by getting rid of largely unproductive photogenerated holes in the valence band and electrons in the conduction band. However, this electric field is not very helpful in creating oxidative species because the energy potential of these charge carriers is not high enough. Instead, the remaining charge carriers that are effective in photochemical reactions have a potent redox ability, such as the ability to create ($\dot{O}_2^-$) through reduction reactions and ($\dot{O}H$) through oxidation potential. Afterward, the MnO_2 CBs electrons, which have a potent reducing capability, reduce hydrogen ions, leading to the production of H_2. This process follows the S-scheme of electron transfer. When water splits, the oxidation of OH^- at the VBs h^+ of CdS results in the stoichiometric formation of O_2 gas. On the other hand, the introduction of lactic acid has the effect of donating electrons to the hole, which in turn hinders the recombination of electrons and holes. Additionally, when lactic acid undergoes decomposition, it produces $12H^+$ and $3CO_2$. However, when a pure CdS catalyst is present, the activated CB potential for H_2 production is unstable, which results in a low H_2 reduction rate. However, when a catalyst consisting of a CdS@MnO_2 junction is present, electrons induced by light can move efficiently from CdS to MnO_2. This is because MnO_2 is a competent co-catalyst for the reduction of protons, which allows for H^+ to be efficiently reduced, producing H_2. Additionally, when MnO_2 and CdS particles are combined effectively in a core-shell configuration, the junction interface is activated, and the absorption of the sacrificial agent is increased. As a result, the transfer of electrons from CdS to MnO_2 can be enhanced, and the recombination of electrons and holes can be minimized. These effects lead to an improved catalytic activity. Similar work was reported by Hyerim Park using the co-catalysts of 1CoS@2TiO_2 and lactic acid as an electronic sacrificial agent, the hydrogen production reached up to 1945 μmol g^{-1}, compared to single doping of CoS and TiO_2, respectively [86]. Therefore, S-scheme heterojunctions not only enhance the transfer and division of charge carriers but also optimize the redox capabilities of photocatalytic systems [87]. It is easier to create S-scheme heterojunctions because the RP and OP are directly connected without the need for extra redox couples or carrier-transfer tunnels [88]. Because of these distinctive benefits, S-scheme heterojunctions have found use in various significant photocatalytic processes, including water splitting for H_2 production [89].

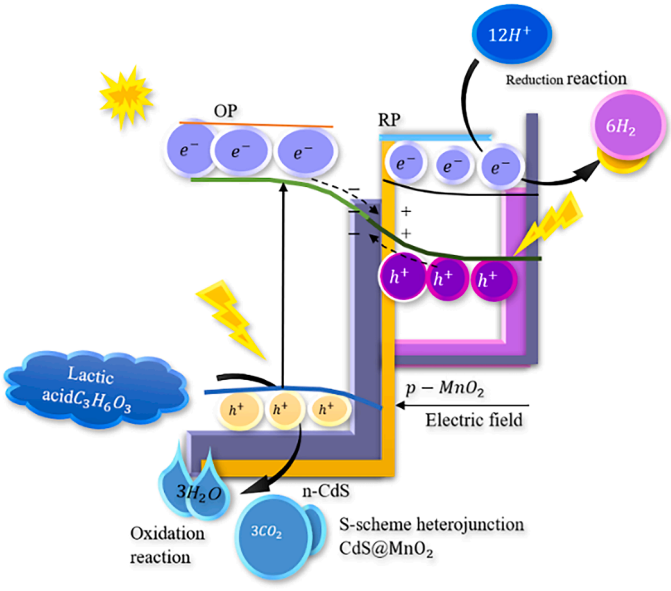

Fig. 8. Schematic of S-scheme charges transfer mechanism on the CdS@MnO_2 particles.

8.1.5. *Creating a p-n heterojunction*

Establishing p-n heterojunction by combining the n-type CdS with a p-type semiconductor is a suitable technique to enhance the stability and photocatalytic effectiveness of CdS. This generates an internal electric field in the vicinity of the p-n junction, creating a positively charged region for the n-type semiconductor and a negatively charged region for the p-type semiconductor. When exposed to light, the photogenerated charge carriers in both the p-type and n-type semiconductors are efficiently separated in space by the internal electric field near the p-n junction. Additionally, as a result of hole transfer from the valence band of the n-type CdS to that of the p-type semiconductor, the CdS becomes enriched with electrons. This leaves behind fewer holes to oxidize the CdS, leading to a decrease in photo corrosion [90].

J. F. D. Reber and M. Rusek managed to create a p-n heterojunction between CdS nanorods and NiS nanoparticles, which demonstrated a considerably greater rate of photocatalytic hydrogen production compared to CdS alone and even CdS loaded with 1 wt% of Pt [90]. The reason for this enhanced performance is due to the formation of a p-n heterojunction that promoted the transfer of charge and inhibited the recombination of charge carriers. Furthermore, the oxidation reaction of S^{2-} and SO_3^{2-} with holes occurred predominantly on the surface, which served as a protective layer for CdS, significantly mitigating photo corrosion.

9. Problem associated with photocatalytic hydrogen production and possible solution

Owing to the numerous methods adopted and technological advancement, there are still a number of challenges associated with photocatalytic H_2 production. The responsible factors include; (i) interfacial charge transfer inhibition (ii) charge carrier recombination (iii) oxidation-reaction. These processes have the potential to reduce the photocatalysis effectiveness usually when exposed to visible spectrum [91]. The solution to photocatalytic H_2 production is:

i. On using the co-catalysts doped photocatalysts improve photocatalytic activity by modifying the electronic structure and reducing the bandgap [92].
ii. To overcome the defects of semiconductors which include interstitial states, which can be able to widen the sunlight near the visible light region [93].
iii. The use of sacrificial reagents is crucial in enhancing photocatalytic performance, which is typically influenced by both the physical and chemical characteristics of the photocatalyst. Most reagents for photocatalytic H_2 production are classified into two main categories, such as the organic compounds comprising

alcohol, hydrocarbons, and organic acids acting as scavengers (i.e., e-donors). In general, sacrificial reagents such as crude glycerol, methanol, glycerol, ethanol, tri-ethanolamine, and lactic acid are commonly utilized. Adding a small amount of these reagents as e-donors can react with the valence band holes generated by light, leading to an increase in the photogenerated electrons. This ultimately enhances the efficiency of hole neutrality, resulting in greater quantum efficiencies [94].

Likewise, inorganic sacrificial agents e.g., Na_2S, Na_2SO_3, Na_2SO_4, $Na_2S_2O_3$, $Na_2S_2O_8$, TEOA are also used as best reagent sulfide based photocatalysts for hydrogen production. They tend to serve as hole scavengers. However, inorganic salts tent to prevent the photo-corrosive nature of the metal sulfides (CdS, MoS, ZnS, etc.) [95]. Na_2S/Na_2SO_3 is used as a sacrificial agent because during photocatalytic reactions, photogenerated electrons on the CB reduce water to produce H_2, while photogenerated holes on the VB oxidize S^{2-} and SO_3^{2-} to form S_2^{2-} and SO_4^{2-} respectively. The holes cannot fully oxidize CdS photocatalysts until the sacrificial reagent is completely used. The resulting S_2^{2-}contributes somewhat to the light absorption of the photocatalyst. The results reported from the literature have shown that CdS-based photocatalysts alone exhibited low H_2 production activity and the least activity performed was 4900 $\mu molg^{-1}h^{-1}$. Therefore, the use of co-catalysts is also important to enhance the use of visible light and overcome the problem of photogenerated charge carriers, thereby promoting the H_2 production activity, which can be observed in Table 2.

The stability of photocatalytic H_2 production for CdS-based photocatalysts with the support of graphene nanocomposites was successfully reviewed. In Table 3 it is clear that ZnS/rGO presents the optimum photocatalytic H_2 production rate of 24,930 $\mu molg^{-1}h^{-1}$ with 8.7-fold enhancement. This is attributed to the sacrificial reagent used, compared to the less H_2 production rate of 500 $\mu molg^{-1}h^{-1}$ obtained. The observed excellent photocatalytic activity attributed to the different types of composites used.

In Table 4, numerous MXene co-catalysts were prepared by different strategies. The photocatalytic activity of MXene supported CdS@TiO_2 core shell revealed an optimum H_2 production rate of 16,200 μmol $h^{-1}g^{-1}$. This may be ascribed to the charge carrier separation enhancement as well as the structural properties. Further addition of defect MoS_2/Ti_3C_2@CdS via hydrothermal method upsurged the catalytic activity which exhibited excellent H_2 production around 14,100 μmol h^{-1} g^{-1}, with the enhancement of 18.5, 12.4, and 1.2 higher than that of CdS, Ti_3C_2/CdS and defect MoS_2/CdS, respectively. This result is ascribed to the excellent electrical conductivity of MXene which transfer electron faster. Incorporation of the defect MoS_2 overcomes the recombination of electron and hole pair and offers more active site. The result established that defect MoS_2/Ti_3C_2 play an important role in photocatalytic H_2 production [100], compared to Ti_3C_2/ZIS photocatalysts with the accumulation of layer with H_2 rate of 8.93 μmol h^{-1} g^{-1} and 7.320 enhancement which is higher than that of CdS respectively [14]. However, CdS@Ti_3C_2 MXene exhibited a low H_2 production rate of 1730 μmol h^{-1} g^{-1} compared to the ones reported, this attributed to the increasing content of MXene [104].

The comparison between other semicondoctor materials loading on CdS-based photocatalysts as shown in Table 5. The result presented indicated that CdS/Zn/g-C_3N_4 gives the best result and was achieved with the help of TEOA as a sacrificial reagent the H_2 production rate of 8870 $\mu molg^{-1}h^{-1}$ was recorded compared to the ones presented [108]. Furthermore, the comparison shows that the incorporation of g-C_3N_4/$ZnFe_2O_4$ on CdS hindered the photocatalytic activity and lessened the H_2 production rate to 165 $\mu molg^{-1}h^{-1}$, this is mainly attributed to the use of different sacrificial reagents [109].

The comparison of CdS-based photocatalysts-supported transition metals is described in Table 6. Metal oxides, sulfides, selenide, and phosphide were investigated and considered as excellent co-catalysts due to their great photocatalytic capability. Xing-Liang Yin. et al. reported that the incorporation of Ni_2P@CdS composite shows an excellent photocatalytic stability with a H_2 production rate of 44,650 $\mu molg^{-1}h^{-1}$ by a factor of 127 compared to that of pure CdS was reported and this is due to the optimization of Ni_2P@CdS heterostructure [18]. It was revealed that the synthesized Ni_2P@CdS inhibited the recombination between electron and hole which lessened the involved electrons in the reaction of H^+ reduced into H_2. The result also shows that using Na_2S/Na_2SO_3 as a sacrificial reagent and 300 W $\lambda \geq 420$ *nm* light source contributed to excellent photocatalytic stability and activity compared to the other transition metals co-catalysts listed in Table 6.

Metal-organic frameworks (MOFs) a classic porous material with numerous advantages such as strong adsorption capacity, tailorable structure, and high specific surface area these make them widely accepted in the field of photocatalysis. The H_2 production performance of samples prepared via MOFs is displayed in Table 7 below. It can be also observed that the samples prepared with CdS@Zr-MOF-S displayed low H_2 activity of 1861.7 μmol g^{-1} h^{-1}, this attributed to the use of lactic acid as a sacrificial reagent, whereby the highest H_2 produced observed from CdS@Co_4S_3 was 12,360 μmol g^{-1} h^{-1} and 26 folds enhancement this attributed to the loading of co-catalysts.

10. Conclusion

In conclusion, a recent advancement in the modification of CdS coupled with co-catalysts for efficient solar fuel (H_2) production has been systematically reviewed and discussed. The upcoming efforts for efficient and effective photocatalytic water splitting can be addressed. A well-designed heterostructured significantly suppresses the charge carrier recombination rates, resulting in higher photocatalytic activity. Moreover, adding oxygen transfer reagent eliminates oxygen that causes CdS photocorrosion. In addition, we apply oxygen transfer reagents (AG or PFDL) to remove nascent O_2 from water to prevent oxygen-leading CdS photocorrosion and inhibit the hydrogen and oxygen recombination back into the water. By these strategies, CdS-based semiconductors achieved satisfied stability for photocatalytic overall water splitting under visible light irradiation.

The review recommended that the CB of the co-catalyst should be more negative than that of the photocatalyst so that the photoexcited would move from the CB of the co-catalyst to the photocatalyst semiconductors. In photocatalytic application, CdS-based heterojunctions have potential due to their suitable bandgap and great characteristics, particularly in the photochemical aspect. Therefore, coupling CdS with other supportive co-catalysts will be an important approach for generating based CdS heterojunctions. However, the types of photocatalytic

Table 2
Represents CdS-based single photocatalysts for photocatalytic hydrogen production.

Photocatalysts	Co-catalyst	Sacrificial agent	Light source	H_2 generated	Enhancement (folds)	Ref.
CdS	–	Na_2S/Na_2SO_3	350 W ($\lambda \geq 420$ *nm*)	2155 $\mu molg^{-1}h^{-1}$	3.1	[96]
CdS	–	Lactic acid	300 W($\lambda \geq 420$ *nm*)	4900 μmol h^{-1} g^{-1}	–	[31]
CdS	–	Na_2S/Na_2SO_3	300 W($\lambda \geq 420$ *nm*)	180 $\mu molh^{-1}$	–	[97]
CdS	–	Lactic acid	300 W ($\lambda \geq 400$ *nm*)	330 μmol g^{-1} h^{-1}	–	[98]

Table 3
Comparison of solar fuel hydrogen production of CdS-based material/graphene composite.

Photocatalysts	Co-catalyst	Sacrificial agent	Light source	H_2 generated (μmol g^{-1} h^{-1})	Enhancement (folds)	Ref.
CdS	Ni/GO	Ethanol	4 W ($\lambda \geq 420$ *nm*)	8866	–	[99]
CdS	rGO	Na_2S/Na_2SO_3	300 W ($\lambda \geq$ 420 *nm*)	500	–	[100]
CdS	rGO/ZnO	Lactic acid	300 W ($\lambda \geq$ 420 *nm*)	10,550	–	[101]
CdS	Ni@graphene	TEOA	300 W ($\lambda \geq$ 420 *nm*)	5900	–	[102]
CdS	ZnS/rGO	Na_2S/Na_2SO_3	300 W ($\lambda \geq$ 420 *nm*)	24,930	87.4	[103]

Table 4
Comparison of solar fuel (hydrogen) production of CdS-based material supported MXene.

Photocatalysts	Co-catalyst	Sacrificial agent	Light source	H_2 generated (μmol g^{-1} h^{-1})	Enhancement (folds)	Ref.
CdS	Ti_3C_2 MXene	Lactic acid	350 W($\lambda \geq 420$ *nm*)	88.162	91.57	[105]
CdS	Ti_3C_2 MXene	–	300 W ($\lambda > 420$ nm)	1730	–	[104]
CdS	MoS_2/Ti_3C_2	Lactic acid	300 W ($\lambda > 420$ nm)	14,100	18.5	[106]
CdS	@TiO_2/ Mxene	Lactic acid	300 W ($\lambda > 420$ nm)	16,200	–	[107]
CdS	Ti_3C_2/ZIS	triethanolamine	300 W ($\lambda > 420$ nm	8930	7.32	[14]

Table 5
Comparison of solar fuel (hydrogen) production of CdS-based material.

Photocatalysts	Co-catalyst	Sacrificial agent	Light source	H_2 generated (μmol$g^{-1}h^{-1}$)	Enhancement (folds)	Ref.
CdS	g-C_3N_4	Lactic acid	300 W ($\lambda \geq 420$ *nm*)	392.84	–	[110]
CdS	g-$C_3N_4/ZnFe_2O_4$	Na_2SO_3/Na_2S	300 W($\lambda \geq$ 420 *nm*)	405	45	[109]
CdS	Zn/g-C_3N_4	TEOA	300 W ($\lambda \geq 420$ *nm*)	8870	3.46	[108]
CdS	g-C_3N_4-GA	TEOA	300 W ($\lambda \geq 420$ *nm*)	8638	2–3	[111]
CdS	Ni_3S_2/Cu_2S	Na_2S/Na_2SO_3	300W($\lambda \geq 420$ *nm*)	568.1	1.8	[112]
CdS	α-Fe_2O_3/CdS/g-C_3N_4	Na_2S/Na_2SO_3	1000 W xenon lamp	165	–	[113]

Table 6
Represent CdS-based photocatalyst with metal oxides, sulfides, selenide, and phosphide.

Photocatalysts	Co-catalyst	Sacrificial agent	Light source	H_2 generated (μmol$g^{-1}h^{-1}$)	Enhancement (folds)	Ref.
CdS	$Fe_xCo_{1-x}P$	$(NH_4)_2SO_3$	300 W ($\lambda \geq 420$ *nm*)	18,270	–	[114]
CdS	CoS/	lactic acid	300 W ($\lambda \geq 420$ *nm*)	3193.7	32	[115]
CdS	Cu_2MoS_4	Lactic acid	150 W	15,560	4.2	[116]
CdS	MoS/	Na_2S/Na_2SO_3	300 W ($\lambda > 420$ nm)	2300	8	[117]
CdS	ZnO	Na_2S/Na_2SO_3	150 W ($\lambda > 420$ nm)	4076	76.91	[98]
CdS	MoS	Lactic acid	500 W	5240	–	[118]
CdS	$Cu_{1.81}S$	Na_2S/Na_2SO_3	300 W	2714	150	[119]
CdS	Co	$(NH_4)_2SO_3$	($\lambda > 420$ nm)	1299	17	[120]
CdS	Ni_2P	Na_2S/Na_2SO_3	300 W ($\lambda \geq 420$ *nm*)	44,650	127	[18]
CdS	ZnO/MoS_2	Na_2S/Na_2SO_3	300 W ($\lambda \geq 420$ *nm*)	10,247.4	30.7	[121]
CdS	MoS_2	Lactic acid	3000 W $\lambda \geq 420$ nm	13,600	–	[69]
CdS	ZnSe	Ethylenediamine		3818.7	–	[122]
CdS	Pt/CdS@Al_2O_3	Lactic acid		62.1	–	[15]

principles were described pointing to the semiconductor heterojunction schemes such as the Z-scheme and S- scheme photocatalysts. It is revealed from the review that S-scheme photocatalysts offer a great advantage in H_2 production via converting and transferring photo-generated carriers. Hence, utilization of the S-scheme can significantly improve the production of H_2 respectively.

CRediT authorship contribution statement

Dahiru Umaru: Conceptualization, Data curation, Investigation, Methodology, Writing – original draft, Writing – review & editing. **Hafeez Yusuf Hafeez:** Conceptualization, Data curation, Funding acquisition, Investigation, Methodology, Resources, Supervision, Validation, Visualization, Writing – review & editing, Project administration. **J. Mohammed:** Conceptualization, Data curation, Formal analysis, Investigation, Methodology, Project administration, Resources, Supervision, Writing – review & editing, Validation, Visualization. **Abdussalam Balarabe Suleiman:** Conceptualization, Methodology, Project administration, Resources, Supervision, Validation, Visualization. **Chifu Ebenezer Ndikilar:** Conceptualization, Formal analysis, Investigation,

Table 7
Comparison of solar fuel (hydrogen) production of CdS-based material supported MOFs.

Photocatalysts	Co-catalyst	Sacrificial agent	Light source	H_2 generated (μmol g^{-1} h^{-1})	Enhancement (folds)	Ref.
CdS	Co_4S_3	Lactic acid	150 W ($\lambda \geq 420$ nm)	12,360	26	[123]
CdS	Co_4S_3 (0.2)	Lactic acid	300 W ($\lambda \geq 420$ nm)	5892.6	–	[124]
CdS	Ni-MOF	Na_2SO_4	300 W ($\lambda \geq 420$ nm)	2508	8	[125]
CdS	MoS_2	Na_2S/Na_2SO_3	300 W ($\lambda \geq 420$ nm)	3318	10	[126]
CdS	Zr-MOF-S	lactic acid	300 W ($\lambda \geq 420$ nm)	1861.7	4.5	[127]
CdS	Ti@Zr	Na_2S/Na_2SO_3	300 W ($\lambda \geq 420$ nm)	78.9	–	[128]
CdS	C-Ni_2P@MOFs	Na_2S/Na_2SO_3	300 W ($\lambda \geq 540$ nm)	28,391	11	[129]

Methodology, Project administration, Resources, Supervision, Validation, Visualization, Writing – review & editing. **Yusuf Zakariyya:** Data curation, Methodology, Writing – review & editing.

Declaration of Competing Interest

The authors declare that they have no known competing financial interests or personal relationships that could have appeared to influence the work reported in this paper.

Data availability

Data will be made available on request.

Acknowledgements

This document has been produced with the financial assistance of the European Union (Grant no. DCI-PANAF/2020/420-028), through the African Research Initiative for Scientific Excellence (ARISE), pilot program. ARISE is implemented by the African Academy of Sciences with support from the European Commission and the African Union Commission. The contents of this document are the sole responsibility of the author(s) and can under no circumstances be regarded as reflecting the position of the European Union, the African Academy of Sciences, and the African Union Commission.

References

[1] Q. Wang, Q. Gao, A.M. Al-Enizi, A. Nafady, S. Ma, Recent advances in MOF-based photocatalysis: environmental remediation under visible light, Inorg. Chem. Front. 7 (2) (2020) 300–339, https://doi.org/10.1039/C9QI01120J.
[2] E.I. Epelle, K.S. Desongu, W. Obande, A.A. Adeleke, P.P. Ikubanni, J .A. Okolie, B. Gunes, A comprehensive review of hydrogen production and storage: a focus on the role of nanomaterials, Int. J. Hydrogen Energy 47 (47) (2022) 20398–20431, https://doi.org/10.1016/j.ijhydene.2022.04.227.
[3] M. Bai, K. Song, Y. Sun, M. He, Y. Li, J. Sun, An overview of hydrogen underground storage technology and prospects in China, J. Pet. Sci. Eng. 124 (2014) 132–136, https://doi.org/10.1016/j.petrol.2014.09.037, 2014.
[4] N.T. Stetson, S. McWhorter, C.C. Ahn, Introduction to hydrogen storage, in: R. B. Gupta, A. Basile, T.N. Veziroğlu (Eds.), Compendium of Hydrogen Energy, Woodhead Publishing, 2016, pp. 3–25, https://doi.org/10.1016/B978-1-78242-362-1.00001-8, 2.
[5] R. Li, X. Ou, L. Zhang, Z. Oi, X. Wu, C. Lu, J. Fan, K. Lv, Photocatalytic oxidation of NO on reduction type semiconductor photocatalysts: effect of metallic Bi on CdS nanorods, Chem. Commun. 57 (78) (2021) 10067–10070, https://doi.org/10.1039/D1CC03516A.
[6] H. Long, P. Wang, X. Wang, F. Chen, H. Yu, Optimizing hydrogen adsorption of NixB cocatalyst by integrating P atom for enhanced photocatalytic H_2-production activity of CdS, Appl. Surf. Sci. 604 (2022), https://doi.org/10.1016/j.apsusc.2022.154457.
[7] A. Kumar, S. Rana, T. Wang, P. Dhiman, G. Sharma, B. Du, F.J. Stadler, Advances in S-scheme heterojunction semiconductor photocatalysts for CO_2 reduction, nitrogen fixation and NOx degradation, Mater. Sci. Semicond. Process. 168 (2023), 107869, https://doi.org/10.1016/j.mssp.2023.107869.
[8] K. Wu, C. Wu, W. Bai, N. Li, Y. Gao, L. Ge, CdS supported on ZIF-67-derived Co-N-C as efficient nano polyhedron photocatalysts for visible light induced hydrogen production, Colloids Surfaces A 18 (663) (2023), 131089, https://doi.org/10.1016/j.colsurfa.2023.131089R.
[9] H.B. Huang, Z.B. Fang, K. Yu, J. Lü, R. Cao, Visible-light-driven photocatalytic H_2 evolution over CdZnS nanocrystal solid solutions: interplay of twin structures sulfur vacancies and sacrificial agents, J. Mater. Chem. A 8 (7) (2020) 3882–3891, https://doi.org/10.1039/C9TA13836F.
[10] S. Liu, M.Q. Yang, Z.R. Tang, Y.J. Xu, A nanotree-like CdS/ZnO nanocomposite with spatially branched hierarchical structure for photocatalytic fine-chemical synthesis, Nanoscale 6 (13) (2014) 7193–7198, https://doi.org/10.1039/C4NR01227E.
[11] L. Huang, X. Wang, J. Yang, G. Liu, J. Han, C. Li, Dual cocatalysts loaded type I CdS/ZnS core/shell nanocrystals as effective and stable photocatalysts for H_2 evolution, J. Phys. Chem. C 117 (22) (2013) 11584–11591, https://doi.org/10.1021/jp400010z. Jun.
[12] L.J. Zhang, S. Li, B.K. Liu, D.J. Wang, T.F. Xie, Highly efficient CdS/WO_3 photocatalysts: z-scheme photocatalytic mechanism for their enhanced photocatalytic H_2 evolution under visible light, ACS Catal 4 (10) (2014) 3724–3729, https://doi.org/10.1021/cs500794j. Oct.
[13] T. Kim, H. Park, B. Hyung Park, S. Joon Yoon, C. IU, S. Woo Joo, N. Son, M. Kang, Long-term catalytic durability in Z-scheme CdS @ 1T-WS_2 heterojunction materials, J. Ind. Eng. Chem. 105 (2022) 337–351, https://doi.org/10.1016/j.jiec.2021.09.035.
[14] J. Bai, W. Chen, R. Shen, Z. jiang, P. Zhang, W. Liu, X. Li, Regulating interfacial morphology and charge-carrier utilization of Ti_3C_2 modified all-sulfide CdS/$ZnIn_2S_4$ S-scheme heterojunctions for effective photocatalytic H_2 evolution, J. Mater. Sci. Technol. 112 (2022) 85–95, https://doi.org/10.1016/j.jmst.2021.11.003.
[15] X. Ning, W. Zhen, Y. Wu, G. Lu, Inhibition of CdS photocorrosion by Al_2O_3 shell for highly stable photocatalytic overall water splitting under visible light irradiation, Appl. Catal. B Environ. 226 (2018) 373–383, https://doi.org/10.1016/j.apcatb.2017.12.067.
[16] W. Zhen, X. Ning, M. Wang, Y. Wu, G. Lu, Enhancing hydrogen generation via fabricating peroxide decomposition layer over NiSe/MnO_2-CdS catalyst, J. Catal. 367 (2018) 269–282, https://doi.org/10.1016/j.jcat.2018.09.019.
[17] J. Zhang, Y. Wang, J. Jin, J. Zhang, Z. Lin, F. Huang, J. Yu, Efficient visible-light photocatalytic hydrogen evolution and enhanced photostability of core/shell CdS/g-C_3N_4 nanowires, ACS Appl. Mater. Interfaces 5 (20) (2013) 10317–10324, https://doi.org/10.1021/am403327g. Oct.
[18] X.L. Yin, L. Lei-Lei, Han Shu-Rui, D. Xin-Xin, P. Dong-Hui, Wang Min, Li Da-Cheng, Dou Jian-Min, Green and in-situ synthesis of noble-metal-free Ni_2P/CdS nanoheterostructure for enhanced photocatalytic H_2 generation activity, J. Taiwan Inst. Chem. Eng. 103 (2019) 110–117, https://doi.org/10.1016/j.jtice.2019.08.001.
[19] Y. Wang, S. Feng, X. Cao, Synthesis of Z-type heterojunction bifunctional composites with Mn-doped CdS nanoparticles supported on NH_2-MIL-125 (Ti) for hydrogen evolution and antibiotic degradation under visible light, Opt. Mater. 135 (2022), 113087, https://doi.org/10.1016/j.optmat.2022.113087, 2023.
[20] R. Gao, L. Xiong, L. Huang, W. Chen, X. Li, X. Liu, L. Mao, A new structure of Pt NF@Ni(OH)$_2$/CdS heterojunction: preparation, characterization and properties in photocatalytic hydrogen generation, Chem. Eng. J. 430 (2022), 132726, https://doi.org/10.1016/j.cej.2021.132726.
[21] C. Bie, B. Zhu, L. Wang, H. Yu, C. Jiang, T. Chen, J. Yu, A bifunctional CdS/MoO_2/MoS2 catalyst enhances photocatalytic H_2 evolution and pyruvic acid synthesis, Angew. Chemie Int. Ed. 61 (44) (2022), 202212045, https://doi.org/10.1002/anie.202212045.
[22] Y.J. Yuan, D. Chen, Z.T. Yu, Z.G. Zou, Cadmium sulfide-based nanomaterials for photocatalytic hydrogen production, J. Mater. Chem. A 6 (25) (2018) 11606–11630, https://doi.org/10.1039/C8TA00671G.
[23] Q. Li, X. Li, and J. Yu, "Surface and interface modification strategies of CdS-based photocatalysts". 31(2020), doi: 10.1016/B978-0-08-102890-2.00010-5.
[24] R. Banerjee, R. Jayakrishnan, P. Ayyub, Effect of the size-induced structural transformation on the band gap in CdS nanoparticles, J. Phys. Condens. Matter. 12 (50) (2000) 10647–10654, https://doi.org/10.1088/0953-8984/12/50/325.
[25] Y. Cao, J. Wang, One-Pot synthesis of high-quality zinc-blende CdS nanocrystals, J. Am. Chem. Soc. 126 (2004) 14336–14337, https://doi.org/10.1021/ja0459678.

[26] Y. Nakaoka, Y. Nosaka, Electron spin resonance study of radicals produced on irradiated CdS powder, J. Phys. Chem. 99 (24) (1995) 9893–9897, https://doi.org/10.1021/j100024a035.

[27] A.V. Rane, K. Kanny, V.K. Abitha, and S. Thomas, "Methods for Synthesis of Nanoparticles and Fabrication of Nanocomposites," in Synthesis of Inorganic Nanomaterials, 121–139, 2018, doi: https://doi.org/10.1016/B978-0-08-101975-7.00005-1.

[28] K. Byrappa, Novel hydrothermal solution routes of advanced high melting nanomaterials processing, J. Ceram. Soc. Japan 117 (1363) (2009) 236–244, https://doi.org/10.2109/jcersj2.117.236.

[29] A. Billah, F. Tojo, S. Kubota, F. Hirose, B. Ahmmad, Organic molecule embedded CdS nanocomposite for hydrogen generation from water: effect of precursors' concentrations, Int. J. Hydrogen Energy 46 (71) (2021) 35302–35310, https://doi.org/10.1016/j.ijhydene.2021.08.100.

[30] J. Wang, J. Yang, H. Yang, H. Huang, X. Yang, L. Wei, Solvothermal synthesis of CdS at different solvents and its photocatalytic activity for antibiotics, Opt. Mater. (Amst). 135 (2022), 113303, https://doi.org/10.1016/j.optmat.2022.113303, 2023.

[31] Z.Ai.G. Zhao, Y. Zhong, Y. Shao, B. Huang, Y. Wu, X. Hao, Phase junction CdS: high efficient and stable photocatalyst for hydrogen generation, Appl. Catal. B Environ. 221 (2017) 179–186, https://doi.org/10.1016/j.apcatb.2017.09.002, 2018.

[32] F. Dong, L. Qin, T. Zhang, X. Li, S. Kang, A novel pathway toward efficient improvement of the photocatalytic activity and stability of CdS- based photocatalyst for light driven H_2 evolution : the synergistic effect between CdS and $SrWO_4$, Int. J. Hydrogen Energy 48 (7) (2022) 13877–13889, https://doi.org/10.1016/j.ijhydene.2022.12.289.

[33] I. Bekri-Abbes, E. Srasra, Investigation of structure and conductivity properties of polyaniline synthesized by solid–solid reaction, J. Polym. Res. 18 (4) (2011) 659–665, https://doi.org/10.1007/s10965-010-9461-x.

[34] K. Maeda, K. Teramura, D. Lu, T. Takata, N. Saito, Y. Inoue, K. Domen, Photocatalyst releasing hydrogen from water, Nature 440 (7082) (2006) 295, https://doi.org/10.1038/440295a.

[35] Y. Li, Y. Cao, D. Jia, A general strategy for synthesis of metal nanoparticles by a solid-state redox route under ambient conditions, J. Mater. Chem. A 2 (11) (2014) 3761–3765, https://doi.org/10.1039/C3TA14427E.

[36] Z. Xu, R. Chu, J. Hao, G. Li, Q. Yin, Citrate-oxide method to prepare $SrBi_4Ti_4O_{15}$ powders and ceramics, J. Alloys Compd. 479 (1) (2009) 500–504, https://doi.org/10.1016/j.jallcom.2008.12.094.

[37] Y. Dimitriev, Y. Ivanova, R. Iordanova, History of sol-gel science and technology, J. Univ. Chem. Technol. Metall. 43 (2008) 181–192.

[38] A.E. Danks, S.R. Hall, Z. Schnepp, The evolution of 'sol–gel' chemistry as a technique for materials synthesis, Mater. Horiz. 3 (2) (2016) 91–112, https://doi.org/10.1039/C5MH00260E.

[39] W.T. Yao, S.H. Yu, S.J. Liu, J.P. Chen, X.M. Liu, F.Q. Li, Architectural control syntheses of CdS and CdSe nanoflowers, branched nanowires, and nanotrees via a solvothermal approach in a mixed solution and their photocatalytic property, J. Phys. Chem. B 110 (24) (2006) 11704–11710, https://doi.org/10.1021/jp060164n. Jun.

[40] A.K. Rai, K.K. Jat, Sol-gel synthesis of quantum dots, INC (2023) 35–52, https://doi.org/10.1016/B978-0-12-824153-0.00003-3.

[41] S. Li, et al., Construction of shallow surface states through light Ni doping for high-efficiency photocatalytic hydrogen production of CdS nanocrystals, Chem. – A Eur. J. 20 (1) (2014) 311–316, https://doi.org/10.1002/chem.201302679.

[42] B. Rheingans, E.J. Mittemeijer, Modelling precipitation kinetics: evaluation of the thermodynamics of nucleation and growth, Calphad 50 (2015) 49–58, https://doi.org/10.1016/j.calphad.2015.04.013.

[43] V. Preethi, S. Kanmani, Photocatalytic hydrogen production using Fe_2O_3-based core shell nano particles with ZnS and CdS, Int. J. Hydrogen Energy 39 (4) (2014) 1613–1622, https://doi.org/10.1016/j.ijhydene.2013.11.029.

[44] X. Ning, J. Li, B. Yang, W. Zhen, Z. Li, B. Tian, Inhibition of photocorrosion of CdS via assembling with thin film TiO_2 and removing formed oxygen by artificial gill for visible light overall water splitting, Appl. Catal. B Environ. 212 (2017) 129–139, https://doi.org/10.1016/j.apcatb.2017.04.074.

[45] H. Dabhane, S. Ghoteker, P. Tambate, S. Pansambal, H.C. Ananda Murthy, R. Oza, Vijay Medhane, A review on environmentally benevolent synthesis of CdS nanoparticle and their applications, Environ. Chem. Ecotoxicol. 3 (2021) 209–219, https://doi.org/10.1016/j.enceco.2021.06.002.

[46] A. Henglein, Photo-Degradation and fluorescence of colloidal-cadmium sulfide in aqueous solution, Berichte der Bunsengesellschaft für Phys. Chemie 86 (4) (1982) 301–305, https://doi.org/10.1002/bbpc.19820860409.

[47] B. Strahlenchemie, "Modern Trends of Colloid Science in Chemistry and Biology 1985 Birkhäuser Verlag Basel," 126–127, 1985.

[48] X. Ning, G. Lu, Photocorrosion inhibition of CdS-based catalysts for photocatalytic overall water splitting, Nanoscale 12 (3) (2020) 1213–1223, https://doi.org/10.1039/c9nr09183a.

[49] C. Wang, L. Wang, J. Jin, J. Liu, Y. Li, M. Wu, L. Chen, B. Wang, X. Yang, L. Su, Probing effective photocorrosion inhibition and highly improved photocatalytic hydrogen production on monodisperse PANI@CdS core-shell nanospheres, Appl. Catal. B Environ. 188 (2016) 351–359, https://doi.org/10.1016/j.apcatb.2016.02.017.

[50] X. Ning, W. Zhen, Y. Wu, G. Lu, Inhibition of CdS photocorrosion by Al_2O_3 shell for highly stable photocatalytic overall water splitting under visible light irradiation, Appl. Catal. B Environ. 226 (2017) 373–383, https://doi.org/10.1016/j.apcatb.2017.12.067, 2018.

[51] C. Lu, E. Wu, C. Li, W. Dou, Y. Lian, Y. Liang, X. Xiang, H. Wang, CoNi bimetallic alloy cocatalyst-modified g-C_3N_4 nanosheets for efficient photocatalytic hydrogen production, J. Phys. Chem. Solids 158 (2021), 110228, https://doi.org/10.1016/j.jpcs.2021.110228.

[52] L. Clarizia, D. Spasiano, I. Di Somma, R. Marotta, R. Andreozzi, D.D. Dionysiou, Copper modified-TiO_2 catalysts for hydrogen generation through photoreforming of organics. A short review, Int. J. Hydrogen Energy 39 (30) (2014) 16812–16831, https://doi.org/10.1016/j.ijhydene.2014.08.037.

[53] W. Gao, Y. Wu, G. Lu, 980nm NIR light driven overall water splitting over a combined CdS–RGO–$NaYF_4$–Yb^{3+}/Er^{3+} photocatalyst, Catal. Sci. Technol. 10 (8) (2020) 2389–2397, https://doi.org/10.1039/D0CY00256A.

[54] D.I. Kondarides, V.M. Daskalaki, A. Patsoura, X.E. Verykios, Hydrogen production by photo-induced reforming of biomass components and derivatives at ambient conditions, Catal. Letters 122 (1) (2008) 26–32, https://doi.org/10.1007/s10562-007-9330-3.

[55] X. Ning, W. Zhen, X. Zhang, G. Lu, Assembly of ultra-thin NiO layer Over $Zn_{1-x}Cd_xS$ for stable visible-light photocatalytic overall water splitting, ChemSusChem 12 (7) (2019) 1410–1420, https://doi.org/10.1002/cssc.201802926.

[56] B. Tian, B. Yang, J. Li, Z. Li, W. Zhen, Y. Wu, G. Lu, Water splitting by CdS/Pt/WO_3-CeO_x photocatalysts with assisting of artificial blood perfluorodecalin, J. Catal. 350 (2017) 189–196, https://doi.org/10.1016/j.jcat.2017.03.012.

[57] P. Hota, A. Das, D.K. Maiti, A short review on generation of green fuel hydrogen through water splitting, Int. J. Hydrogen Energy 48 (2) (2022) 523–541, https://doi.org/10.1016/j.ijhydene.2022.09.264.

[58] N.M. Gupta, Factors affecting the efficiency of a water splitting photocatalyst: a perspective, Renew. Sustain. Energy Rev. 71 (2017) 585–601, https://doi.org/10.1016/j.rser.2016.12.086.

[59] N. Fajrina, M. Tahir, A critical review in strategies to improve photocatalytic water splitting towards hydrogen production, Int. J. Hydrogen Energy 44 (2) (2018) 540–577, https://doi.org/10.1016/j.ijhydene.2018.10.200.

[60] V. Navakoteswara, P. Ravi, M. Sathish, Metal chalcogenide-based core/shell photocatalysts for solar hydrogen production : recent advances, properties and technology challenges, J. Hazard. Mater. 415 (2021), 125588, https://doi.org/10.1016/j.jhazmat.2021.125588.

[61] Y. Luo, Z. Zhang, M. Chhowalla, B. Liu, Recent advances in design of electrocatalysts for high-current-density water splitting, Adv. Mater. 34 (16) (2022), 2108133, https://doi.org/10.1002/adma.202108133.

[62] P. Strasser, K. Shirlaine, T. Anniyey, J.P. Greeley, K.L. More, C. Yu, Z. Liu, Lattice-strain control of the activity in dealloyed core–shell fuel cell catalysts, Nat. Chem. 2 (6) (2010) 454–460, https://doi.org/10.1038/nchem.623.

[63] K.C.S. Lakshmi, B. Vedhanarayanan, T.W. Lin, Electrocatalytic hydrogen and oxygen evolution reactions: role of two-dimensional layered materials and their composites, Electrochim. Acta 447 (2022), 142119, https://doi.org/10.1016/j.electacta.2023.142119, 2023.

[64] X. Xiao, L. Yang Wenping Sun, Y. Chen, Hai Yu, Kangkang Li, Baohua Jia, Lei Zhang, T. Ma, Electrocatalytic water splitting: from harsh and mild conditions to natural seawater, Small 18 (11) (2022), 2105830, https://doi.org/10.1002/smll.202105830.

[65] K. Liu, J. Li, Y. Liu, M. Wang, H. Cui, Dual metal atom catalysts: advantages in electrocatalytic reactions, J. Energy Chem. 79 (2023) 515–534, https://doi.org/10.1016/j.jechem.2023.01.021.

[66] J. Rodríguez, E. Amores, CFD modeling and experimental validation of an alkaline water electrolysis cell for hydrogen production, Processes 8 (12) (2020), https://doi.org/10.3390/pr8121634.

[67] Y.S. Chang, M. Choi, M. Baek, P.Y. Hsieh, K. Yong, Y.J. Hsu, CdS/CdSe co-sensitized brookite H:TiO_2 nanostructures: charge carrier dynamics and photoelectrochemical hydrogen generation, Appl. Catal. B Environ. 225 (2018) 379–385, https://doi.org/10.1016/j.apcatb.2017.11.063.

[68] M.Z. Rahman, M.G. Kibria, C.B. Mullins, Metal-free photocatalysts for hydrogen evolution, Chem. Soc. Rev. 49 (6) (2020) 1887–1931, https://doi.org/10.1039/C9CS00313D.

[69] A. Mehta, A. Misha, S. Basu, N.P. Sheetti, K. Raghava Reddy, T.A. Saleh, T. M. Aminabhavi, Band gap tuning and surface modification of carbon dots for sustainable environmental remediation and photocatalytic hydrogen production–A review, J. Environ. Manage. 250 (2019), 109486, https://doi.org/10.1016/j.jenvman.2019.109486.

[70] M. Antonopoulou, C. Kosma, T. Albanis, I. Konstantinou, An overview of homogeneous and heterogeneous photocatalysis applications for the removal of pharmaceutical compounds from real or synthetic hospital wastewaters under lab or pilot scale, Sci. Total Environ. 765 (2021), 144163, https://doi.org/10.1016/j.scitotenv.2020.144163.

[71] J. Low, J. Yu, M. Jaroniec, S. Wageh, A.A. Al-Ghamdi, Heterojunction photocatalysts, Adv. Mater. 29 (20) (2017), 1601694, https://doi.org/10.1002/adma.201601694.

[72] X. He, T. Kai, P. Ding, Heterojunction photocatalysts for degradation of the tetracycline antibiotic: a review, Environ. Chem. Lett. 19 (6) (2021) 4563–4601, https://doi.org/10.1007/s10311-021-01295-8.

[73] D. Zhu, Z. Dong, F. Lv, C. Zhong, W. Huang, The development of balanced heterojunction photocatalysts, Cell Reports Phys. Sci. 3 (10) (2022), 101082, https://doi.org/10.1016/j.xcrp.2022.101082.

[74] H. Zhou, Y. Qu, T. Zeid, X. Duan, Towards highly efficient photocatalysts using semiconductor nanoarchitectures, Energy Environ. Sci. 5 (5) (2012) 6732–6743, https://doi.org/10.1039/C2EE03447F.

[75] Q. Xiang, J. Yu, M. Jaroniec, Enhanced photocatalytic H_2-production activity of graphene-modified titania nanosheets, Nanoscale 3 (9) (2011) 3670–3678, https://doi.org/10.1039/C1NR10610D.

[76] L. Wang, C. Bie, J. Yu, Challenges of Z-scheme photocatalytic mechanisms, Trends Chem 4 (11) (2022) 973–983, https://doi.org/10.1016/j.trechm.2022.08.008.

[77] L.Z. Wu, B. Chen, Z.J. Li, C.H. Tung, Enhancement of the efficiency of photocatalytic reduction of protons to hydrogen via molecular assembly, Acc. Chem. Res. 47 (7) (2014) 2177–2185, https://doi.org/10.1021/ar500140r. Jul.

[78] P. Hota, A. Das, D.K. Maiti, A short review on generation of green fuel hydrogen through water splitting, Int. J. Hydrogen Energy 48 (2) (2023) 523–541, https://doi.org/10.1016/j.ijhydene.2022.09.264.

[79] A.J. Bard, Photoelectrochemistry and heterogeneous photo-catalysis at semiconductors, J. Photochem. 10 (1) (1979) 59–75, https://doi.org/10.1016/0047-2670(79)80037-4.

[80] H. Zhu, B. Yang, J. Xu, Z. Fu, M. Wen, T. Guo, S. Fu, j. Zuo, S. Zhang, Construction of Z-scheme type CdS–Au–TiO_2 hollow nanorod arrays with enhanced photocatalytic activity, Appl. Catal. B Environ. 90 (3) (2009) 463–469, https://doi.org/10.1016/j.apcatb.2009.04.006.

[81] Q. Xu, L. Zhang, J. Yu, S. Wageh, A.A. Al-Ghamdi, M. Jaroniec, Direct Z-scheme photocatalysts: principles, synthesis, and applications, Mater. Today 21 (10) (2018) 1042–1063, https://doi.org/10.1016/j.mattod.2018.04.008.

[82] S. Chen, D. Huang, P. Xu, W. Xue, L. Lei, M. Cheng, R. Wang, X. Liu, R. Deng, Semiconductor-based photocatalysts for photocatalytic and photoelectrochemical water splitting: will we stop with photocorrosion? J. Mater. Chem. A 8 (5) (2020) 2286–2322, https://doi.org/10.1039/C9TA12799B.

[83] Q. Xu, L. Zhang, B. Cheng, J. Fan, J. Yu, S-scheme heterojunction photocatalyst, Chem 6 (7) (2020) 1543–1559, https://doi.org/10.1016/j.chempr.2020.06.010.

[84] J. Fu, Q. Xu, J. Low, C. Jiang, J. Yu, Ultrathin 2D/2D WO_3/g-C_3N_4 step-scheme H_2-production photocatalyst, Appl. Catal. B Environ. 243 (2019) 556–565, https://doi.org/10.1016/j.apcatb.2018.11.011.

[85] Y. Yang, J. Wu, B. Cheng, L. Zhang, A.A. Al-Ghamdi, Swelm Wageh, Youji Li, Enhanced photocatalytic H_2-production activity of CdS nanoflower using Single Atom Pt and graphene quantum dot as dual cocatalysts, chinese j. struct. chem. 41 (6) (2022) 2206006–2206014, https://doi.org/10.14102/j.cnki.0254-5861.2022-0124.

[86] H. Park, S. Kim, T. Kim, Y. Kim, S. Woo, and M. Kang, "CoS@TiO2 S-scheme heterojunction photocatalyst for hydrogen production from photoinduced water splitting," 319, April 2021.

[87] X. Wang, G. Liu, Z. Gang Chen, F. Li, L. Wang, G. Qing Lu, H. Ming Cheng, Enhanced photocatalytic hydrogen evolution by prolonging the lifetime of carriers in ZnO/CdS heterostructures, Chem. Commun. 23 (2009) 3452–3454, https://doi.org/10.1039/B904668B.

[88] L. Wang, J. Zhang, H. Yu, I.H. Patir, Y. Li, S. Wangeh, A.A. Al-Ghamdi, J. Yu, Dynamics of photogenerated charge carriers in inorganic/organic s-scheme heterojunctions, J. Phys. Chem. Lett. 13 (21) (2022) 4695–4700, https://doi.org/10.1021/acs.jpclett.2c01332. Jun.

[89] L. Wang, B. Zhu, J. Zhang, J.B. Ghasemi, M. Mousavi, J. Yu, S-scheme heterojunction photocatalysts for CO_2 reduction, Matter 5 (12) (2022) 4187–4211, https://doi.org/10.1016/j.matt.2022.09.009.

[90] J.F.D. Reber, M. Rusek, Photochemical hydrogen production with platinized suspensions of cadmium sulfide and cadmium zinc sulfide modified by silver sulfide, J. Phys. Chem. 90 (1986) 824–834.

[91] R. Saravanan, F. Gracia, A. Stephen, Basic Principles, Mechanism, and Challenges of Photocatalysis. Nanocomposites For Visible Light-Induced Photocatalysis, Springer International Publishing, 2017, pp. 19–40, https://doi.org/10.1007/978-3-319-62446-42.

[92] D. Zheng, Y. Xue, J. Wang, P.S. Varbanov, J.J. Klemeš, C. Yin, Nanocatalysts in photocatalytic water splitting for green hydrogen generation: challenges and opportunities, J. Clean. Prod. 414 (2023), 137700, https://doi.org/10.1016/j.jclepro.2023.137700.

[93] Y. Xu, J. Xu, W. Yan, H. Tang, G. Tang, Synergistic effect of a noble metal free MoS_2 co-catalyst and a ternary Bi_2S_3/MoS_2/P_{25} heterojunction for enhanced photocatalytic H_2 production, Ceram. Int. 47 (7) (2021) 8895–8903, https://doi.org/10.1016/j.ceramint.2020.12.010.

[94] G.J. Lai, L. Ming Lyu, Y. Sheng Huang, G. Chi Lee, M. Pei Lu, T. Pyng Perng, M. Yen Lu, Lih Juann Chen, Few-layer WS_2–MoS_2 in-plane heterostructures for efficient photocatalytic hydrogen evolution, Nano Energy 81 (2021), 105608, https://doi.org/10.1016/j.nanoen.2020.105608.

[95] V. Navakoteswara, P. Ravi, and M. Sathish, "Metal chalcogenide-based core/shell photocatalysts for solar hydrogen production : recent advances, properties and technology challenges," 415(2021), 125588, dio: https://doi.org/10.1016/j.jhazmat.2021.125588.

[96] C. Bie, J. Fu, B. Cheng, L. Zhang, Ultrathin CdS nanosheets with tunable thickness and efficient photocatalytic hydrogen generation, Appl. Surf. Sci. 462 (2018) 606–614, https://doi.org/10.1016/j.apsusc.2018.08.130.

[97] W. Kim, D. Monllor-satoca, W. Chae, M.A. Mahadik, J. Suk, Enhanced photoelectrochemical and hydrogen production activity of aligned CdS nanowire with anisotropic transport properties, Appl. Surf. Sci. 463 (2018) 339–347, https://doi.org/10.1016/j.apsusc.2018.08.127, 2019.

[98] S. Huo and C. Chen, "One-step synthesis CdS/single crystal ZnO nanorod heterostructures with high photocatalytic H2 production ability," Inorg. Chem. Commun., 132, 108841, doi: 10.1016/j.inoche.2021.108841.

[99] O. Quiroz-cardoso, S. Oros-ruiz, A. Solís-gómez, R. López, R. Gómez, Enhanced photocatalytic hydrogen production by CdS nanofibers modified with graphene oxide and nickel nanoparticles under visible light, Fuel 237 (2019) 227–235, https://doi.org/10.1016/j.fuel.2018.10.013.

[100] Y. Wang, C. Liu, C. Kong, F. Zhang, Colloids and surfaces A : physicochemical and engineering aspects defect MoS_2 and Ti_3C_2 nanosheets co-assisted CdS to enhance visible-light driven photocatalytic hydrogen production, Colloids Surfaces A Physicochem. Eng. Asp. 652 (2022), 129746, https://doi.org/10.1016/j.colsurfa.2022.129746.

[101] X. Deng, J. Chen, Y. Luo, S. Huo, and C. Chen, "Ce-metal organic framework and reduced graphene oxide co-enhanced the H2 evolution ability of CdS/single crystal ZnO nanorod photocatalyst," Int. J. Hydrogen Energy, 48(92), 35986–35996, doi: 10.1016/j.ijhydene.2023.06.009.

[102] T. Di, L. Zhang, B. Cheng, J. Yu, J. Fan, CdS nanosheets decorated with Ni@graphene core-shell cocatalyst for superior photocatalytic H_2 production, J. Mater. Sci. Technol. 56 (2020) 170–178, https://doi.org/10.1016/j.jmst.2020.03.032.

[103] Z. Yin, M. Li, N. Wang, Z. Zhou, Y. Hu, D. Fan, Y. Pang, Y. Liu, Z. Lu, and J. Hai, "Deposition of CdS and ZnS directly on rGO via . an emulsion-solvothermal method for excellent photocatalytic activity and stability," 612(2022), 155844, doi: 10.1016/j.apsusc.2022.155844.

[104] X. Chen, Y. Guo, R. Bian, Y. Ji, X. Wang, X. Zhang, H. Cui, J. Tian, Titanium carbide MXenes coupled with cadmium sulfide nanosheets as two-dimensional/two-dimensional heterostructures for photocatalytic hydrogen production, J. Colloid Interface Sci. 613 (2022) 644–651, https://doi.org/10.1016/j.jcis.2022.01.079.

[105] Y. Wang, X. Wang, Y. Ji, R. Bian, J. Li, X. Zhang, J. Tian, Q. Yang, F. Shi, Ti_3C_2, "Ti_3C_2 MXene coupled with CdS nanoflowers as 2D/3D heterostructures for enhanced photocatalytic hydrogen production activity, Int. J. Hydrogen Energy 47 (52) (2022) 22045–22053, https://doi.org/10.1016/j.ijhydene.2022.05.014.

[106] Y. Wang, C. Liu, C. Kong, F. Zhang, Defect MoS_2 and Ti_3C_2 nanosheets co-assisted CdS to enhance visible-light driven photocatalytic hydrogen production, Colloids Surfaces A Physicochem. Eng. Asp. 652 (2022), 129746, https://doi.org/10.1016/j.colsurfa.2022.129746.

[107] V. Navakoteswara Rao, H. Kwon, Y. Lee, P. Ravi, C. Won Ahn, K. Kim, J. Mo Yang, Synergistic integration of Mxene nanosheets with CdS@TiO_2 core@shell S-scheme photocatalyst for augmented hydrogen generation, Chem. Eng. J. 471 (2023), 144490, https://doi.org/10.1016/j.cej.2023.144490.

[108] H. Li, S. Tao, S. Wan, G. Qiu, Q. Long, J. Yu, S. Cao, S-scheme heterojunction of ZnCdS nanospheres and dibenzothiophene modified graphite carbon nitride for enhanced H_2 production, Chinese J. Catal. 46 (2023) 167–176, https://doi.org/10.1016/S1872-2067(22)64201-3.

[109] R. Belakehal, K. Atacan, A. Megriche, and M. Ozacar, "Fabrication of heterostructured CdS/g-C3N4/ZnFe2O4 nanocomposite synthesized through ultrasonic-assisted method for efficient photocatalytic hydrogen production," 602 (2022), 154315 doi: 10.1016/j.apsusc.2022.154315.

[110] G. Li, H. Liang, G. Xu, C. Li, J. Bai, Controllable synthesized heterojunction hollow nanotube of g-C_3N_4/CdS: enhance visible light catalytic performance for hydrogen production, J. Phys. Chem. Solids 145 (2020), dd109549, https://doi.org/10.1016/j.jpcs.2020.109549.

[111] Y. Liu, J. Sun, X. Zhou, Y.Zhou C.Lv, B. Cong, G. Chen, An in-plane S-scheme heterostructure drives H_2 production with water and solar energy, Chem. Eng. J. 437 (1) (2022), 135280, https://doi.org/10.1016/j.cej.2022.135280.

[112] M. Sun, Q.huang X.Guan, Q. Gao, S. Zhang, X. Cai, Y. Fang, F. Peng, S. Yang, CdS@Ni_3S_2/Cu_2S electrode for electrocatalysis and boosted photo-assisted electrocatalysis hydrogen production, Ceram. Int. 319 (2023), 124085, https://doi.org/10.1016/j.seppur.2023.124085. www.elsevier.com/locate/seppur.

[113] C. Yavuz, S. Erten-ela, Solar light-responsive α-Fe_2O_3/CdS/g-C_3N_4 ternary photocatalyst for photocatalytic hydrogen production and photodegradation of methylene blue, J. Alloys Compd. 908 (2022), 164584, https://doi.org/10.1016/j.jallcom.2022.164584.

[114] J. Zhang, Q. Zhao, J. Zhang, Y. Shi, C. Huang, Highly active $Fe_xCo_{1-x}P$ cocatalysts modified CdS for photocatalytic hydrogen production, Int. J. Hydrogen Energy 45 (43) (2020) 22722–22731, https://doi.org/10.1016/j.ijhydene.2020.06.090.

[115] L. Shen, J. Cheng, X. Wang, H. Wang, Z. Lu, L. Guo, H. Ma, L. Li, H. Wen, Inorganica chimica acta fabrication of CoS/CdS heterojunctions for enhanced photocatalytic hydrogen production, Inorganica Chim. Acta 541 (2022), 121085, https://doi.org/10.1016/j.ica.2022.121085.

[116] S. Hong, D.P. Kumar, D.A. Reddy, J. Choi, T.K. Kim, Excellent photocatalytic hydrogen production over CdS nanorods via using noble metal-free copper molybdenum sulfide (Cu_2MoS_4) nanosheets as co-catalysts, Appl. Surf. Sci. 396 (2017) 421–429, https://doi.org/10.1016/j.apsusc.2016.10.171.

[117] H. Liu, P. Tan, Y. Liu, H. Zhai, W. Du, X. Liu, J. Pan, Ultrafast interfacial charge evolution of the Type-II cadmium Sulfide/Molybdenum disulfide heterostructure for photocatalytic hydrogen production, J. Colloid Interface Sci. 619 (2022) 246–256, https://doi.org/10.1016/j.jcis.2022.03.080.

[118] X. Zhou, J. Huang, H. Zhang, H. Sun, W. Tu, Controlled synthesis of CdS nanoparticles and their surface loading with MoS_2 for hydrogen evolution under visible light, Int. J. Hydrogen Energy 41 (33) (2016) 14758–14767, https://doi.org/10.1016/j.ijhydene.2016.06.190.

[119] S. Liu, X. Guo, W. Wang, Y. Yang, C. Zhu, Environmental CdS-$Cu_{1.81}$S-heteronanorods with continuous sublattice for photocatalytic hydrogen production, Appl. Catal. B Environ. 303 (2021), 120909, https://doi.org/10.1016/j.apcatb.2021.120909, 2022.

[120] W. Chen, Y. Wang, M. Liu, L. Gao, L. Mao, Z. Fan, W. Shangguan, In situ photodeposition of cobalt on CdS nanorod for promoting photocatalytic hydrogen production under visible light irradiation, Appl. Surf. Sci. 444 (2018) 485–490, https://doi.org/10.1016/j.apsusc.2018.03.068.

[121] Y. Jia, Z. Wang, X. Qing Qiao, L. Huang, S. Gan, D. Hou, J. Zhao, C. Snu, D. Sheng Li, A synergistic effect between S-scheme heterojunction and Noble-metal free

cocatalyst to promote the hydrogen evolution of ZnO/CdS/MoS_2 photocatalyst, Chem. Eng. J. 424 (2021), 130368, https://doi.org/10.1016/j.cej.2021.130368.
[122] M. Chen, P. Wu, Y. Zhu, S. Yang, Enhanced photocatalytic H_2 production activity of CdZnS with stacking faults structure assisted by ethylenediamine and NiS, Int. J. Hydrogen Energy 43 (24) (2018) 10938–10949, https://doi.org/10.1016/j.ijhydene.2018.04.218.
[123] D.P. Kumar, H. Park, E. Hwa Kim, S. Hong, M. Gopannagari, D. Amaranatha, Reddy, T. Kyu Kim, Environmental Noble metal-free metal-organic framework-derived onion slice-type hollow cobalt sulfide nanostructures: enhanced activity of CdS for improving photocatalytic hydrogen production, Appl. Catal. B Environ. 224 (2017) 230–238, https://doi.org/10.1016/j.apcatb.2017.10.051, 2018.
[124] R. Huang, W. Chen, y. Zhang, Z. Huang, Y. Zhou, Y. Wu, X. Lv, Two dimensional metal-organic frameworks-derived leaf-like Co_4S_3/CdS composite for enhancing photocatalytic water evolution, J. Colloid Interface Sci. 554 (2019) 39–47, https://doi.org/10.1016/j.jcis.2019.06.098.
[125] J. Guo, Y. Liang, L. Liu, J. Hu, H. Wang, W. An, W. Cui, Noble-metal-free CdS/Ni-MOF composites with highly efficient charge separation for photocatalytic H_2 evolution, Appl. Surf. Sci. 522 (2020), 146356, https://doi.org/10.1016/j.apsusc.2020.146356.
[126] S. Liu, Y. Yang, W. Xiao, S. Xia, C. Jin, W. Wang, S. Li, M. Zhong, S. Wang, C. Chen, Metal-organic frameworks derived porous MoS_2/CdS heterostructure for efficient photocatalytic performance towards hydrogen evolution and organic pollutants, Int. J. Hydrogen Energy 48 (84) (2023) 32729–32738, https://doi.org/10.1016/j.ijhydene.2023.05.050, 1–10.
[127] H. Hu, K. Zhang, G. Yan, L. Shi, B. Jia, H. Hunang, Y. Zhang, X. Sun, T. Ma, Precisely decorating CdS on Zr-MOFs through pore functionalization strategy : a highly efficient photocatalyst for H_2 production, Chinese J. Catal. 43 (9) (2022) 2332–2341, https://doi.org/10.1016/S1872-2067(21)63949-9.
[128] W. Hou, M. Chen, C. Chen, Y. Wang, Y. Xu, Increased production of H_2 under visible light by packing CdS in a Ti, Zr-Based metal organic framework, J. Colloid Interface Sci. 604 (2021) 310–318, https://doi.org/10.1016/j.jcis.2021.06.150.
[129] C. Zhang, S. Chu, B. Liu, Y. Liu, Z. Guo, Z. Lv, MOF-mediated fabrication of coralloid Ni_2P@CdS for enhanced visible-light hydrogen evolution, Appl. Surf. Sci. 569 (2021), 150987, https://doi.org/10.1016/j.apsusc.2021.150987.